Structures 79 (2025) 109364

Contents lists available at ScienceDirect

Structures

journal homepage: www.elsevier.com/locate/istruc

Geometric amplification of damping: Novel mechanisms for enhanced vibration control

Sondipon Adhikari, Sudip Chowdhury*

Glasgow Computational Engineering Centre, James Watt School of Engineering, The University of Glasgow, Glasgow G12 8QQ, United Kingdom

ARTICLE INFO

Keywords:
Ordinary damping amplifiers
Compound damping amplifiers
Nested damping amplifiers
Levered damping amplifiers

ABSTRACT

This paper introduces damping amplifiers as an innovative solution to enhance the vibration reduction capabilities of conventional base isolators while addressing their inherent limitations. Four distinct classes of damping amplifiers are presented: ordinary damping amplifiers, compound damping amplifiers, nested damping amplifiers, and levered damping amplifiers. The governing equations of motion for these damping amplifiers and their corresponding damping amplifier base isolators are derived using Newton's second law. H_∞ optimisation method is utilised to obtain exact closed-form expressions for the optimal design parameters of these novel isolators. A comprehensive parametric study is conducted by applying the optimal design parameters, demonstrating that damping amplifiers can amplify the effective damping of isolators by a factor of 1000 compared to conventional isolators, without introducing additional static damping into the dynamic systems. The transfer matrix is formulated to analyse the dynamic responses of isolated structures in the frequency domain, while the time history analysis is performed to validate the frequency domain results. The Newmark-beta method is mathematically integrated with isolator design to evaluate the time history results under real earthquake ground motions. Results indicate that the novel isolators exhibit an improvement of 84.22 % in performance over conventional isolators. All results are mathematically verified, ensuring the validity of the findings.

1. Introduction

The vibration of engineering dynamic systems is governed by their mass, stiffness, and damping properties. Therefore, the control of vibration is essentially achieved by manipulating the mass, stiffness, and damping of a dynamic system, either separately or together. Over the years, engineers have introduced and perfected innovative technologies for controlling these properties. The control of stiffness properties is generally easier and most abundant in practice. This can be achieved by advanced materials such as composites and honeycombs. Alternatively, active materials such as piezoelectric materials and shape memory alloys can be used to manipulate stiffness properties as necessary.

Controlling the mass, on the other hand, is more challenging than controlling the stiffness. This is because most materials have an inherent density, which is generally difficult to alter. Smith [1] introduced an innovative way to manipulate mass through an inerter [2]. The concept used rotating flywheels, and effectively, this can be viewed as a separate element representing a higher mass without actually increasing the physical mass [3]. Initial works on inerters involved noise and vibration reduction in automobiles [4]. Later, inerters have been used for vibration absorption [5]. More recently, inerters have been used for vibration energy harvesting [6]. We refer to a recent review paper by Kuhnert et al. [7] for a comprehensive review of current and historical perspectives on using inerters in dynamic systems [8]. Realising the classical inerter [1] using a flywheel-gear mechanism is conventional [9]. In addition to the classical inerter introduced by Smith, recent research has significantly advanced its applications and structural integrations. For example, Marian and Giaralis explored tuned mass-damper-inerter systems for harmonic vibration suppression and energy harvesting [10]. Lazar et al. demonstrated the use of inerter-based devices for structural vibration suppression [11], while Sun and Lei explored the role of inerters in generating band gaps and dynamic attenuation in periodic structures [12]. Nonlinear inerter configurations have also been investigated in the context of seismic isolation and resilient design [13]. These studies illustrate the versatility of inerter-like devices in passive control strategies [14]. In contrast to these inertia-based systems, the present study proposes a fundamentally different class of damping amplifier mechanisms that achieve enhanced energy dissipation through

* Corresponding author.
Email addresses: Sondipon.Adhikari@glasgow.ac.uk (S. Adhikari), Sudip.Chowdhury@glasgow.ac.uk (S. Chowdhury).

https://doi.org/10.1016/j.istruc.2025.109364
Received 27 January 2025; Received in revised form 4 May 2025; Accepted 2 June 2025
Available online 11 June 2025

geometric motion amplification, without increasing inertial mass. The key distinction lies in the use of linkage mechanisms and lever systems that amplify damper motion, offering an alternative route to effective vibration suppression. A different and simple route to inertial enhancement is using an inertial amplification mechanism [15]. This is achieved through a link-bar mechanism loaded with symmetric masses and a spring. Like the classical inerter, an inertial amplifier also delivers an increased effective mass without increasing the static mass. Inertial amplifiers [16] are mechanisms that augment the effective inertia of a system without proportionally increasing its static mass [17]. They are commonly referred to as mass amplification devices [18], which focus on utilising inertial properties to amplify forces or movements. This approach usually involves using the concepts of mechanical leverage [17], resonance, or inertia to amp up small input forces or displacements into bigger, more usable outputs. The functions and applications of these devices are explained in detail below: Inertial amplifiers work as mass amplification devices by amplifying minute input forces through the use of a mass's inertia. This is often achieved by mechanical configurations that leverage the inertia of a larger mass to produce a proportionately higher force or displacement [19]. These devices are capable of applying mechanical leverage, which is the process by which a set of levers or gears increases the force applied over a longer distance from a smaller force applied over a shorter distance. An alternative tactic is resonance, where a system is designed to oscillate at a particular frequency [20]. Small periodic pressures applied at the resonance frequency have the potential to increase the oscillations in the system and thus amp up the input. By assisting in the measurement and control of vibrations in machinery and buildings, these tools lessen damage and improve engineering performance. Inertial amplifiers have been used for vibration absorption [21], attenuation [22] and low-frequency band-gaps [18,23].

For most practical problems, it is generally necessary to reduce the vibration. This can be achieved by increasing the damping of the system. Like the inertial properties, manipulation of damping is difficult as the physical origin of damping in materials is often poorly understood. The viscous damping model is typically used to model damping [24]. It is possible to consider non-viscous [25,26] or viscoelastic [27,28] damping in the context of vibration reduction. Although advanced damping modelling methods are available, controlling damping in materials is still an open research problem. Therefore, dynamic analysis often uses a discrete damper with a specific damping coefficient. There are also many realistic situations (e.g., automotive suspension, tuned mass dampers) where discrete dampers are used. The damping coefficient can be changed in the analysis for design purposes. In practical terms, a damper with a higher damping coefficient means a larger and heavier damper. It would be practically useful if a smaller damper could deliver a higher damping, similar to an inerter, which delivers a higher mass compared to its actual mass.

Inspired by the ideas of inerters and inertial amplifiers, this paper aims to investigate the possibility of mechanical systems capable of amplifying damping. Although inertial amplifiers have been demonstrated to be very efficient for vibration isolation, their impact on the inherent damping of the system is indirect. A key goal is developing designs that directly enhance a system's damping. In particular, we ask the following fundamental question:

- Can a usual damper attached to a conventional single-degree-of-freedom (SDOF) dynamic system be employed in novel ways such that the effective damping of the system is increased?

This vital question can be addressed from different perspectives. One option is to consider viscoelastic damping, which can be achieved by combining springs and dampers in a combination of series and parallel connections (for example, the classical Biot model [29,30]). This is a mechanical way to enhance damping. The resulting system can be modelled using various techniques, such as damping kernel functions [31,32], fractional derivative models [33], and the GHM model [34,35]. Several innovative mechanical configurations have previously been proposed to enhance structural damping under seismic loading. Notably, Constantinou et al. introduced the toggle-brace-damper system [36,37], demonstrating effective force amplification using a toggle mechanism [38]. Similarly, Sigaher and Constantinou proposed the scissor-jack-damper system [39], which uses a scissor mechanism to amplify damper displacements [39]. Experimental validation of scissor-jack-based energy dissipation systems has been demonstrated by Rama Raju et al. [40], who studied their integration with magnetorheological dampers in a three-storey steel moment-resisting frame. Their results confirmed the potential of such hybrid systems to enhance seismic performance through controlled energy dissipation. Walsh et al. [41] conducted a dynamic analysis of a flexible truss tower equipped with scissor-jack dampers under seismic excitation. Their study highlighted the effectiveness of scissor-jack mechanisms in improving structural response in flexible systems, particularly under dynamic loading conditions. More recently, Yang et al. [42] proposed a novel spatial configuration of the scissor-jack-damper system aimed at enhancing energy dissipation efficiency. This spatial variant demonstrates the continued evolution of linkage-based damping devices and their adaptability to complex structural geometries. More recently, Baquero Mosquera et al. presented an amplification system for concentrated and distributed energy dissipation devices aimed at seismic energy management [43]. These pioneering studies laid the groundwork for damping amplification through geometric configurations. Building upon these foundational concepts, the present study introduces four novel classes of damping amplifiers, ordinary, compound, nested, and levered, with analytically derived damping amplification factors. The methodology employs H_∞ control theory for rigorous optimisation and yields closed-form solutions for isolator design, enabling effective performance comparisons and practical deployment. This paper also addresses the above-mentioned question using a mechanical approach. Novel-specific linkage mechanisms to exploit their movements for enhancing the 'stretching' of a damper and consequently generating more effective damping are introduced in this paper. This fundamental concept can be realised in different ways, which is the focus of this work. This paper proposes four competing mechanisms. It will be shown that, under certain design choices, mechanical systems can amplify effective damping, resulting in a higher damping factor with the same damper. In addition, the proposed damping amplifiers are designed to be integrated into the internal configuration of conventional base isolators without altering the isolator's size or increasing the damper's physical damping coefficient to enhance effective dynamic damping. The structural implementation of this integration is discussed in detail in Section 3 (see Fig. 9). Accordingly, four novel isolators, namely, Ordinary damping-amplifier base isolator, Compound damping-amplifier base isolator, Nested damping-amplifier base isolator, and Levered damping-amplifier base isolator, are introduced in this paper. The governing equations of motion of all dynamic systems are derived using Newton's second law. H_∞ optimisation approach is employed to derive the exact closed-form expressions of these novel isolators. The transfer matrix is formulated to analyse the dynamic responses of isolated structures in the frequency domain, while the time history analysis is performed to validate the frequency domain results. The Newmark-beta method is mathematically integrated with isolator design to evaluate the time history results under real earthquake ground motions. The effectiveness of the advanced damping amplifier designs is validated by comparing the vibration mitigation performance of the novel isolators against that of conventional isolators.

2. Structural model and equations of motion

The concept of damping amplifiers is developed in this section. Four types of damping amplifiers are introduced and mathematically analysed in the following subsections.

2.1. The ordinary damping amplifier

In Fig. 1, the conventional damped single-degree-of-freedom (SDOF) model, the ordinary damping amplifier, and the corresponding free-body diagram are shown. This mechanism is similar to the conventional iner-

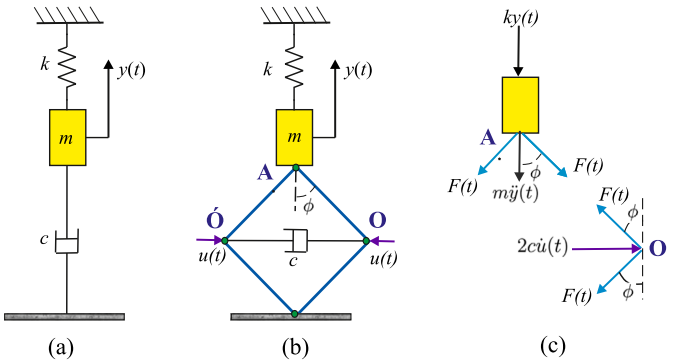

Fig. 1. The conventional damped single-degree-of-freedom (SDOF) model, the ordinary ideal damping amplifier, and the free-body diagram. (a) The mass, stiffness, and damping of the SDOF oscillator are given by m, k, and c, respectively. (b) The ordinary damping amplifier is obtained by inserting a damper within a rhombus mechanism made of four rigid links. The amplifier angle is ϕ, and the amplifier damping is c. (c) The free-body diagram for the ordinary damping amplifier. The displacement of the mass (at point A) and the amplifier damper (at point O) are denoted by $y(t)$ and $u(t)$, respectively. The force $F(t)$ is the internal force within the rigid links.

tial amplifier extensively discussed in the literature [17]. This damping amplifier is reviewed here for the purpose of comparing and contrasting on a similar footing with the models to be introduced later.

The damper in the conventional damped SDOF model and the damping amplifier SDOF model are exactly the same. The damper in the amplifier is placed horizontally within a rhombus mechanism made of four rigid links. The amplifier angle is ϕ with respect to the vertical line, and it is assumed that the rhombus mechanism can move freely in a friction less manner about the four hinges marked in Fig. 1(b) by green dots. The free-body diagram for the ordinary damping amplifier is shown in Fig. 1(c). The displacement of the mass (at point A) and the amplifier damper (at point O) are denoted by $y(t)$ and $u(t)$, respectively. The motions $y(t)$ and $u(t)$ are perpendicular to each other. The force $F(t)$ is the internal force within the rigid links. Note that due to the symmetry of the mechanism, the dynamics at points O and O' are the same. Therefore, it is sufficient to consider the dynamic equilibrium at one point only.

The equation of motion of free vibration of the conventional SDOF is given by

$$m\ddot{y}(t) + ky(t) + c\dot{y}(t) = 0 \tag{1}$$

Dividing by the mass, the equation of motion can be rewritten as

$$\ddot{y}(t) + \omega_n^2 y(t) + 2\zeta\omega_n \dot{y}(t) = 0 \tag{2}$$

Here the undamped natural frequency (ω_n) and the damping factor (ζ) are expressed as

$$\omega_n = \sqrt{\frac{k}{m}} \tag{3}$$

$$\text{and} \quad \frac{c}{m} = 2\zeta\omega_n \quad \text{or} \quad \zeta = \frac{c}{2\sqrt{km}} \tag{4}$$

One of the main objectives of the damping amplifier is to alter the effective damping factor of the SDOF system in Fig. 1(b) without changing the damper. To obtain the equation of motion, considering the equilibrium of the mass from point A in the free-body diagram in Fig. 1(c), we have

$$m\ddot{y}(t) + ky(t) + 2F(t)\cos\phi = 0 \tag{5}$$

Here $F(t)$ is the internal force within the rigid link bars. The damper is compressed by $2u(t)$ between the points O and O'. Balancing the force arising from the motion of the damper from the equilibrium at point O, we have

$$2F(t)\sin\phi - 2c\dot{u}(t) = 0 \tag{6}$$

The vertical motion of point O is $y(t)/2$ due to the vertical symmetry of the mechanism. Considering the bars in Fig. 1(b) are rigid, using the kinematic relationship of the rigid bars, one deduces

$$\frac{y(t)}{2}\cos\phi = u(t)\sin\phi \quad \text{or} \quad u(t) = y(t)\cot\phi/2 \tag{7}$$

Substituting this in Eq. (6) we have

$$2F(t)\sin\phi = c\cot\phi\dot{y}(t) = 0 \quad \text{or} \quad 2F(t) = c\frac{\cot\phi}{\sin\phi}\dot{y}(t) \tag{8}$$

Substituting this in Eq. (5), we obtain the equation of motion as

$$m\ddot{y}(t) + ky(t) + c\cot^2\phi\ \dot{y}(t) = 0 \tag{9}$$

It can be seen that the effective damping of the novel damping amplifier in Fig. 1(b) is $c_a = c\cot^2\phi$. Therefore, we define the damping amplification factor as the ratio of the damping factor of the amplifier to the damping factor of the original system as

$$\mathcal{F}_d = \frac{\zeta_a}{\zeta} = \cot^2\phi \tag{10}$$

Here, ζ_a is the damping factor of the damping amplifier in Fig. 1(b). The damping factor $\mathcal{F}_d$ is the key parameter which quantifies and also characterises the efficiency of a damping amplifier. In Fig. 2, the damping amplification factor is plotted as a function of the amplifier angle ϕ. This is a log plot, and we observe that the damping amplification increases exponentially when the amplifier angle ϕ is closer to zero. This result shows that the theoretical damping amplification can be over 1000 times compared to the conventional SDOF system with the same damper. The two key assumptions made in deriving the equation of motion of the ideal amplifier are: (1) the hinge movements between the four link-bars, the mass, the ground and the damper are frictionless, and (2) the masses of the four link bars are negligible. When the amplifier angle ϕ becomes close to zero, the mechanism becomes extremely narrow, and even very small friction in the hinges will prevent it from

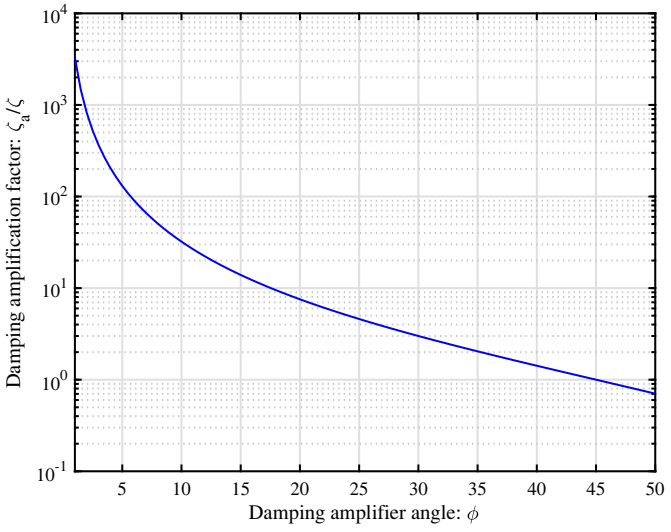

Fig. 2. Damping amplification as a function of the amplifier angle ϕ for the ideal ordinary damping amplifier. For smaller amplifier angles $\phi \lessapprox 20°$, the damping amplification becomes prominent.

operating properly. Keeping this in mind, it is preferable that $\phi \geq 10°$. This will ensure that the assumptions made are applicable to our model. Another point to be noted is that the damping amplifier effectively does not provide any amplification when $\phi > 45°$. Therefore, the amplifier angle should be chosen to be smaller than 45°.

2.2. The compound damping amplifier

The ordinary damping amplifier introduced in the previous section has the potential for enhanced vibration reduction due to the increased effective damping. However, it was observed that its efficiency might be reduced when the amplifier angle ϕ is not small. Therefore, in this section, we explore designs which can provide efficiency over a larger parameter region.

The key idea here is to have multiple smaller damping amplifiers working in unison. The introduced design of a compound damping amplifier with two cells is shown in Fig. 3. Two secondary mechanisms are inserted within a primary mechanism. The primary amplifier angle is ϕ, and the secondary amplifier angle is θ. Each damper within the cells is $c/2$, so the total damping is c, which is the same as the baseline SDOF oscillator. This way, the damping amplification performance can be compared consistently with the previous case.

The displacement of the mass (at point A), point O and the amplifier damper (at point B) are $y(t)$, $u(t)$ and $v(t)$, respectively. From Fig. 3(a), observe that point D is fixed, and point C only moves in the vertical direction due to the symmetry of the system. Therefore, the vertical motion at point O is $y(t)/2$, and the horizontal motion at point B is $u(t)/2$.

Considering the bars in Fig. 3(a) are rigid, using the kinematic relationship of the primary mechanism, one obtains

$$\frac{y(t)}{2}\cos\phi = u(t)\sin\phi \quad \text{or} \quad u(t) = y(t)\cot\phi/2 \tag{11}$$

From the kinematic relationship of the secondary mechanisms, we can deduce that

$$v(t)\cos\theta = \frac{u(t)}{2}\sin\theta \quad \text{or} \quad v(t) = u(t)\tan\theta/2 \tag{12}$$

Combining the preceding two equations, the motion of the damper can be related to the motion of the primary mass as

$$v(t) = \frac{y(t)}{4}\cot\phi\tan\theta \tag{13}$$

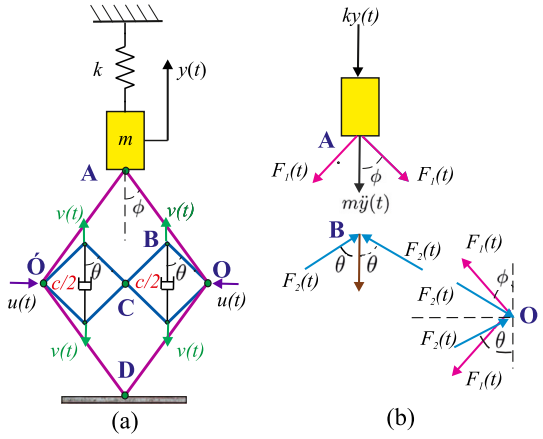

Fig. 3. The compound damping amplifier and its corresponding free-body diagram. (a) A compound damping amplifier with two damping cells. The primary amplifier angle is ϕ, and the secondary amplifier angle is θ. Each damper within the cells is $c/2$ so that the total damping is the same as the baseline SDOF oscillator. (b) The free-body diagram for the compound damping amplifier. The displacement of the mass (at point A), point O and the amplifier damper (at point B) are denoted by $y(t)$, $u(t)$ and $v(t)$ respectively. The forces $F_1(t)$ and $F_2(t)$ are the internal forces within the rigid links of the primary and secondary mechanisms.

The net stretching of the dampers is $2v(t)$. Considering the equilibrium of the forces in the vertical direction, from point B in the free-body diagram in Fig. 3(b), we have

$$2F_2(t)\cos\theta = (c/2)2\dot{v}(t) = c\dot{v}(t) \tag{14}$$

Considering the equilibrium of the forces in the horizontal direction from point O in the free-body diagram, we have

$$2F_1(t)\sin\phi = 2F_2(t)\sin\theta = c\dot{v}(t)\tan\theta \tag{15}$$

$$\text{or} \quad 2F_1(t) = \frac{c\dot{v}(t)\tan\theta}{\sin\phi} = \frac{c\dot{y}(t)\tan^2\theta\cot\phi}{4\sin\phi} \tag{16}$$

Considering the equilibrium of the mass from point A in the free-body diagram, we have

$$m\ddot{y}(t) + ky(t) + 2F_1(t)\cos\phi = 0 \tag{17}$$

Substituting $F_1(t)$ from Eq. (15) into the above equation, we have the equation of motion of an SDOF oscillator with the compound damping amplifier as

$$m\ddot{y}(t) + ky(t) + c\dot{y}(t)\cot^2\phi\frac{\tan^2\theta}{4} = 0 \tag{18}$$

We obtain the damping amplification factor as the ratio of the damping factor of the amplifier to the damping factor of the original system as

$$\mathcal{F}_d = \frac{\zeta_a}{\zeta} = \cot^2\phi\left(\frac{\tan^2\theta}{4}\right) \tag{19}$$

Comparing this to the damping amplification factor of the ordinary amplifier in Eq. (10), we observed that the damping amplification factor of the compound amplifier is $\left(\frac{\tan^2\theta}{4}\right)$ times more. Therefore, the compound amplifier will outperform the ordinary amplifier provided

$$\tan\theta > 2 \quad \text{or} \quad \theta \gtrapprox 64° \tag{20}$$

This requirement, in addition to $\phi < 45°$ required for damping amplification from the ordinary amplifier. The condition that each term be greater than 1.0 was introduced to provide a conservative and straightforward design guideline, ensuring reliable amplification. This approach simplifies the design space and guarantees that the overall amplification factor exceeds unity without relying on delicate parameter balancing.

In Fig. 4, the damping factor of the ideal and compound amplifier are compared. Amplifications for three different values of the secondary amplifier angle θ are shown in the figure. This clearly shows that when $\theta > 64°$, the amplification of the compound amplifier is more than its ordinary counterpart. The results in Fig. 4 also give another interesting possibility which is not available for the ordinary amplifier. For a given target damping amplification, say 100, a range of combinations of ϕ and θ can be selected. This gives more opportunities for the design and satisfies any practical constraints.

2.3. The nested damping amplifier

In the previous section, we showed that the damping amplification can be enhanced by introducing secondary mechanisms within the primary mechanism. Motivated by this, here we take this idea further in the form of a nested damping amplifier design shown in Fig. 5. The amplifier is obtained by introducing two connected four-bar rhombus mechanisms inside the primary mechanism. Overall, the design conceived in Fig. 5 is therefore made up of three mechanisms, and they are marked on the figure. The damper with a damping coefficient c is placed horizontally inside the innermost mechanism. Therefore, the amount of damping employed in the enhancer is the same as the original SDOF system.

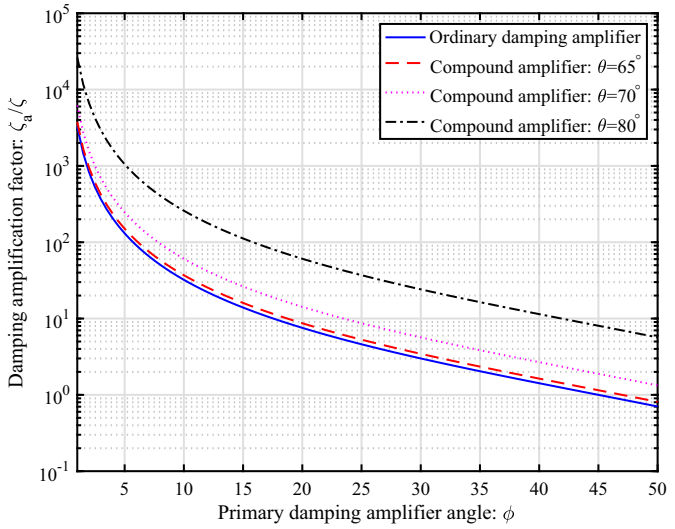

Fig. 4. Damping amplification as a function of the primary amplifier angle ϕ for the compound amplifier SDOF systems for various secondary amplifier angle θ.

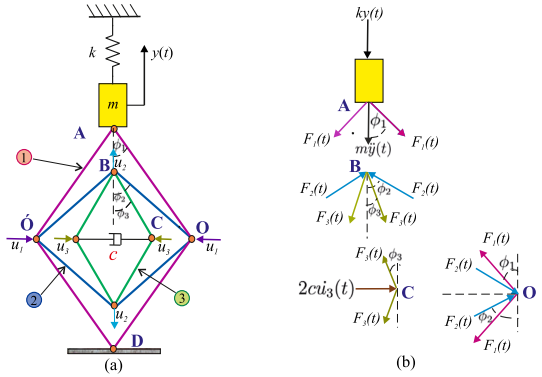

Fig. 5. The nested damping amplifier and its corresponding free-body diagram. (a) The nested damping amplifier is made up of three connected mechanisms. The damper c is placed horizontally inside the innermost mechanism. The amplifier angles for the mechanisms are ϕ_1, ϕ_2 and ϕ_3 as shown. (b) The free-body diagram for the nested damping amplifier. The displacement of the mass (at point A), points O, B and C are denoted by $y(t)$, $u_1(t)$, $u_2(t)$ and $u_3(t)$, respectively. The forces $F_1(t)$, $F_2(t)$ and $F_3(t)$ are the internal forces within the rigid links of mechanisms 1, 2 and 3 respectively.

The amplifier angles for the mechanisms are ϕ_1, ϕ_2 and ϕ_3. The displacement of the mass (at point A), points O, B and C are $y(t)$, $u_1(t)$, $u_2(t)$ and $u_3(t)$, respectively. From Fig. 5(a) observe that point D is fixed and point B only moves in the vertical direction due to the symmetry of the system. Therefore, the vertical motion at point O is $y(t)/2$.

Using the kinematic relationship of mechanism 1, one obtains

$$\frac{y(t)}{2}\cos\phi_1 = u_1(t)\sin\phi_1 \quad \text{or} \quad u_1(t) = y(t)\cot\phi_1/2 \tag{21}$$

Next, we consider the motion of mechanism 2. Considering, for example, that the member OB is of fixed length, we can deduce

$$u_1\sin\phi_2 = u_2\cos\phi_2 \tag{22}$$

Finally, considering the motion of mechanism 3 and noting that the member CB is of fixed length, we obtain

$$u_3\sin\phi_3 = u_2\cos\phi_3 \tag{23}$$

Combining the above three kinematic relationships, the motion of the innermost mechanism containing the damper can be linked with the motion of the primary oscillating mass as

$$u_3 = \frac{y(t)}{2}\cot\phi_1\tan\phi_2\cot\phi_3 \tag{24}$$

Now, we consider the free-body diagram in Fig. 5(b) and investigate the equilibrium at various points to obtain the equation of motion. Considering the equilibrium of the mass from point A in the free-body diagram, we have

$$m\ddot{y}(t) + ky(t) + 2F_1(t)\cos\phi_1 = 0 \tag{25}$$

The net stretching of the damper is $2u_3(t)$. Using the equilibrium of the forces in the horizontal direction from point C in the free-body diagram, we have

$$2F_3(t)\sin\phi_3 = 2c\dot{u}_3(t) \tag{26}$$

From the equilibrium of the forces in the vertical direction, from point B in the free-body diagram, one obtains

$$2F_2\cos\phi_2 = 2F_3\cos\phi_3 \tag{27}$$

Considering the equilibrium of the forces in the horizontal direction from point O in the free-body diagram, we have

$$2F_1(t)\sin\phi_1 = 2F_2(t)\sin\phi_2 \tag{28}$$

Combining Eqs. (23)–(28), the equation of motion of an SDOF oscillator with the nested damping amplifier can be obtained as

$$m\ddot{y}(t) + ky(t) + c\dot{y}(t)\cot^2\phi_1\tan^2\phi_2\cot^2\phi_3 = 0 \tag{29}$$

We obtain the damping amplification factor as the ratio of the damping factor of the amplifier to the damping factor of the original system as

$$\mathcal{F}_d = \frac{\zeta_a}{\zeta} = \cot^2\phi_1\left(\tan^2\phi_2\cot^2\phi_3\right) \tag{30}$$

Comparing this to the damping amplification factor of the ordinary amplifier in Eq. (10), it is noted that the damping amplification factor of the nested amplifier is $\left(\tan^2\phi_2\cot^2\phi_3\right)$ times more. Therefore, the nested amplifier will outperform the ordinary amplifier provided

$$\tan\phi_2 > 1 \quad \text{or} \quad \phi_2 > 45° \quad \text{and} \quad \cot\phi_3 > 1 \quad \text{or} \quad \phi_3 < 45° \tag{31}$$

These requirements are in addition to $\phi_1 < 45°$ necessary for damping amplification from the ordinary amplifier. The condition that each term be greater than 1.0 was introduced to provide a conservative and straightforward design guideline, ensuring reliable amplification. This approach simplifies the design space and guarantees that the overall amplification factor exceeds unity without relying on delicate parameter balancing.

In Fig. 6, the damping factors of the ideal and the nested amplifier are compared. Amplifications for three different values of combinations of the angles ϕ_2 and ϕ_3 are shown. These results clearly show that when $\phi_2 > 45°$ and $\phi_3 < 45°$, the amplification of the nested amplifier is much more than its ordinary counterpart. The results in Fig. 6 also give another interesting possibility, which is not available for the ordinary amplifier. For a given target damping amplification, say 100, a range of combinations of ϕ_1, ϕ_2, and ϕ_3 can be selected. This gives more opportunities for the design and satisfies any practical constraints. The schematic diagrams of the compound and the nested amplifier are drawn in a 2D plane. However, they can be fabricated such that different mechanisms operate at different planes. This way, a wide range of amplifier angles can be achieved without the issue of mechanisms touching each other. In principle, one can add more internal and nested mechanisms following the idea introduced in Figs. 3 and 5. The damping amplification factors

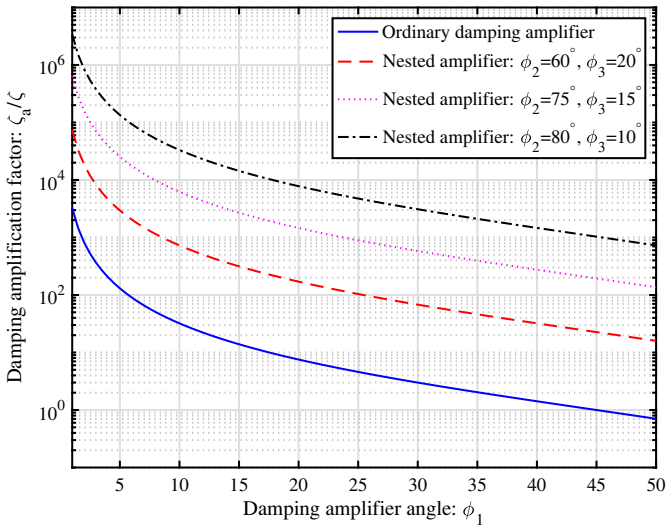

Fig. 6. Damping amplification as a function of the amplifier angle ϕ_1 for the nested amplifier SDOF systems for various combinations of ϕ_2 and ϕ_3.

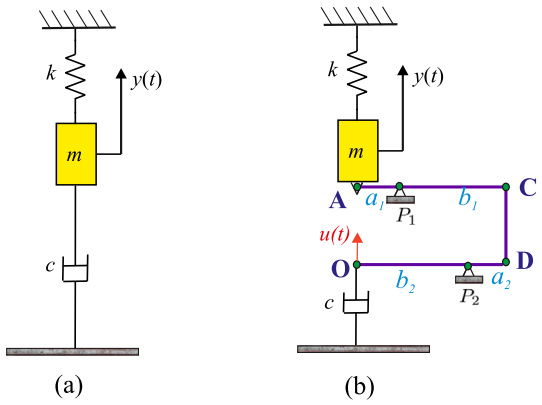

Fig. 7. The conventional damped single-degree-of-freedom (SDOF) model and the levered damping amplifier. (a) The mass, stiffness and damping of the SDOF oscillator are given by m, k and c, respectively. (b) The levered damping amplifier is made up of two connected levers. The damper c is connected with the second lever arm at point O. The lever arm can freely pivot about the points P_1 and P_2.

for such higher-order compounds and nested amplifiers will be more numerous and will follow the same trend as derived in Eqs. (19) and (30). However, care should be taken for practical consideration, as there will be many moving parts in higher-order mechanisms. In practical implementations, the presence of multiple moving parts in compound and nested configurations can be addressed by arranging the mechanisms in parallel planes or using layered assemblies to avoid physical interference. Additionally, the use of precision hinges, low-friction bearings, and modular linkage components can facilitate smooth motion transfer and ensure reliable operation of complex amplifier systems.

The rigid-bar assumption is adopted in the analytical formulation to enable closed-form solutions and highlight the fundamental mechanics of damping amplification. In configurations with high amplification, such as the compound and nested designs, elastic deformation of the bars may influence performance. Nevertheless, the models presented offer a novel and effective framework for understanding and designing damping amplifiers, and they provide a solid foundation for future investigations that may incorporate bar compliance through detailed simulations or experiments.

The proposed amplifier mechanisms are constructed using hinged joints, which are commonly used in linkage systems to allow rotational motion with minimal resistance. These joints preserve the kinematic assumptions used in the analytical formulations and ensure proper relative motion between rigid bars. While detailed joint construction is not included in this theoretical study, the use of idealised hinges is sufficient to demonstrate the feasibility and effectiveness of the proposed mechanisms. The configurations presented form a conceptual framework that can be translated into practical designs using standard mechanical joints and fabrication methods in future implementations.

2.4. The levered damping amplifier

So far, the three damping amplifiers introduced all exploit rhombus-shaped four link-bar mechanisms in a novel manner. Although they are very compact and represent a space-saving design, there are many moving parts. The aim here is to conceive amplifier designs that use relatively simpler mechanisms. The concept of a damping amplifier that uses only mechanical levers is shown in Fig. 7. A damper with damping coefficient c is connected with the second lever arm at point O. The rods AC, CD and DO are assumed to be rigid. In addition, the rod AC pivots freely about P_1, and the rod DO pivots freely about P_2. The rod CD simply connects rods AC and DO and transfers the motion. Considering these, the motion at point O can be obtained as

$$u(t) = \frac{b_1}{a_1}\frac{b_2}{a_2}y(t) \tag{32}$$

Using this, the equation of motion of an SDOF oscillator with the levered damping amplifier can be obtained as

$$m\ddot{y}(t) + ky(t) + F_A(t) = 0 \tag{33}$$

where $F_A(t)$ is the force at point A. This can be related to the force at point O as

$$F_A(t) = \frac{b_1}{a_1}\frac{b_2}{a_2}F_O(t) = \left(\frac{b_1}{a_1}\frac{b_2}{a_2}\right)c\dot{u}(t) = \left(\frac{b_1}{a_1}\frac{b_2}{a_2}\right)^2 c\dot{y}(t) \tag{34}$$

We can obtain the damping amplification factor as the ratio of the damping factor of the amplifier to the damping factor of the original system as

$$\mathcal{F}_d = \frac{\zeta_a}{\zeta} = \left(\frac{b_1}{a_1}\frac{b_2}{a_2}\right)^2 \tag{35}$$

Therefore, provided $b_1 > a_1$ and $b_2 > a_2$, the levered amplifier in Fig. 7 will deliver an increased amplification. For example, when $b_1/a_1 = 2$ and $b_2/a_2 = 3$, the levered amplifier's damping amplification factor will be 36. The damping amplification factor of the levered damping amplifier in Eq. (35) is compared with the ordinary damping amplifier's damping amplification factor, which is expressed in Eq. (10) to obtain the superior damping amplification ability of the levered damping amplifier. The superior damping amplification factor is mathematically formulated and expressed as

$$\begin{aligned}\left(\frac{b_1}{a_1}\frac{b_2}{a_2}\right)^2 &> \cot^2\phi \\ \left(\frac{b_1}{a_1}\frac{b_2}{a_2}\right) &> \pm\cot\phi\end{aligned} \tag{36}$$

The +ve root of Eq. (36) is considered. Fig. 8 shows the requirement of a minimal lever arm ratio to achieve robust performance of levered damping amplifier with the conjunction of damping amplifier angle. The graph indicates that the levered damping amplifier provides more effective damping amplification with a minimal lever-arm ratio than the ordinary one. The damping amplifiers are further installed in the core material of the conventional base isolators in order to boost the vibration reduction capacities of these devices and overcome the limitations

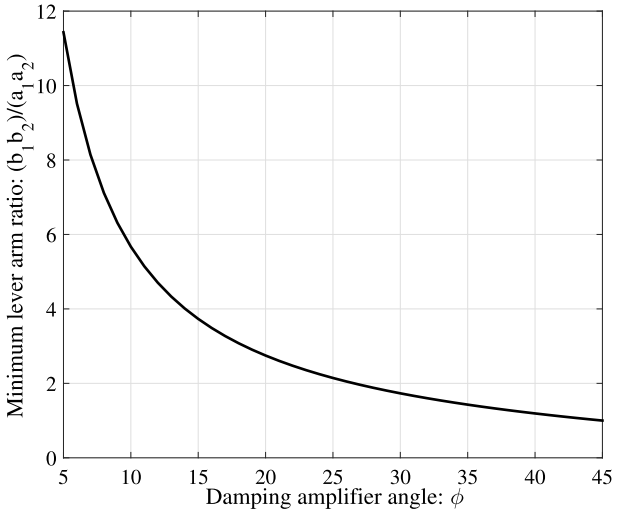

Fig. 8. The minimal lever arm ratio required for the levered damping amplifier to surpass the performance of the ordinary damping amplifier is shown as a function of the damping amplifier angle ϕ.

that they already have. In the following sections, three new classes of damping-amplifier vibration isolation systems are introduced. The four damping amplifier configurations differ significantly in terms of space requirements and damper stroke demands due to their respective linkage mechanisms. Configurations with parallel linkages tend to have a more compact design but may limit the available stroke range, which can reduce damping effectiveness in applications requiring larger travel distances. In contrast, serial linkages and multi-stage systems generally require more space but provide a greater stroke capacity, which is beneficial for applications with higher stroke demands.

In the present study, the levered damping amplifier is introduced as a conceptual model to demonstrate the feasibility of damping amplification through geometric motion transformation. The assumption of rigid levers is made to facilitate analytical tractability and derive closed-form expressions that highlight the core mechanism. While bending flexibility may affect the performance of practical implementations, the theoretical formulation serves as a foundation for further development, including future designs that address stiffness and material constraints through structural optimisation or numerical modelling.

3. Application of damping amplifiers

The structural diagrams of the single degree of freedom systems isolated by the ordinary, compound, nested, and levered damping-amplifier base isolators are subjected to base excitation are shown in Fig. 9(a)–(d). The integration of the proposed damping amplifier mechanisms into base isolators is achieved by embedding them within the internal structure of the isolator, effectively forming a hybrid system that combines conventional isolator components (mass, stiffness, and damping) with geometric amplifier linkages. These amplifiers are configured in such a way that they manipulate the motion of the damper to achieve significantly higher effective damping without increasing the physical size or mass of the isolator itself. As illustrated in Fig. 9, each damping amplifier configuration, such as ordinary, compound, nested, and levered, is incorporated into the isolator's framework, allowing the system to benefit from enhanced energy dissipation while maintaining a compact and practical design. This structural implementation is central to enabling the vibration reduction improvements demonstrated in the subsequent analyses. First, the damping-amplifier enhanced base isolators are designed by applying H_∞ optimisation methods. For this purpose, the amplified isolators are applied at the base of the single degree of freedom systems with the exact amount of mass m_s, stiffness k_s, and damping c_s. The isolated single degree of freedom system is base excited. Newton's second law is applied to derive the governing equations of motion for these isolated SDOF systems. The equation of motion for the novel isolators is derived as

$$m\ddot{y} = -k\left(y - u_g\right) - \tilde{c}\left(\dot{y} - \dot{u}_g\right) + k_s\left(y_s - y\right) + c_s\left(\dot{y}_s - \dot{y}\right) \tag{37}$$

where y and y_s define the absolute displacement of the isolator and SDOF system. u_g defines the base displacement. Now, consider $u = y - u_g$ and $u_s = y_s - y$ and define these degrees of freedom as the relative displacement of the isolator and SDOF system with respect to ground and isolator. After substituting these variables in Eq. (37), this governing equation of motion is rewritten as

$$m\ddot{u} + \tilde{c}\dot{u} + ku - c_s\dot{u}_s - k_s u_s = -m\ddot{u}_g \tag{38}$$

m, $\tilde{c}$, and k define the mass, damping, and stiffness of the damping-amplifier base isolators. For each damping-amplifier base isolator, the value of $\tilde{c}$ has been derived as

Ordinary damping-amplifier base isolator:

$$\tilde{c} = c\underbrace{\cot^2\phi}_{\vartheta} \tag{39}$$

Compound damping-amplifier base isolator:

$$\tilde{c} = c\underbrace{\cot^2\phi\left(\frac{\tan^2\theta}{4}\right)}_{\vartheta} \tag{40}$$

Nested damping-amplifier base isolator:

$$\tilde{c} = c\underbrace{\cot^2\phi_1\tan^2\phi_2\cot^2\phi_3}_{\vartheta} \tag{41}$$

Levered damping-amplifier base isolator:

$$\tilde{c} = c\underbrace{\left(\frac{b_1}{a_1}\frac{b_2}{a_2}\right)^2}_{\vartheta} \tag{42}$$

The value for c has been derived as $c = 2m\xi_d\nu_d$. ϑ defines the damping amplification factor. The governing equation of motion for the isolated SDOF system is derived as

$$m_s\ddot{y}_s = -k_s\left(y_s - y\right) - c_s\left(\dot{y}_s - \dot{y}\right) \tag{43}$$

where y and y_s define the absolute displacement of the isolator and SDOF system. Now, consider $u = y - u_g$ and $u_s = y_s - y$ and define these degrees of freedom as the relative displacement of the isolator and SDOF system with respect to ground and isolator. After substituting these variables in Eq. (43), this governing equation of motion is rewritten as

$$m_s\ddot{u}_s + m_s\ddot{u} + c_s\dot{u}_s + k_s u_s = -m_s\ddot{u}_g \tag{44}$$

where u_g defines the base displacement. The steady state solutions are considered: $u = Ue^{i\omega t}$, $u_s = U_s e^{i\omega t}$, and $\ddot{u}_g = U_g e^{i\omega t}$. These solutions are substituted in Eq. (38) and the last expression of Eq. (44). As a result, a frequency response function has been derived and expressed as

$$\begin{bmatrix} 2i\mu\kappa_d\kappa\xi_d\vartheta + \mu\kappa_d{}^2 - \mu\kappa^2 & -2i\kappa\xi_s - 1 \\ -\kappa^2 & 2i\kappa\xi_s + 1 - \kappa^2 \end{bmatrix}\begin{Bmatrix} U \\ U_s \end{Bmatrix} = -\begin{bmatrix} \mu \\ 1 \end{bmatrix}\frac{U_g}{\nu_s^2} \tag{45}$$

where $\mu = m/m_s$ defines the isolator mass ratio, $\kappa_d = \nu_d/\nu_s$ defines the frequency ratio of the isolator, ξ_d defines the damping ratio of

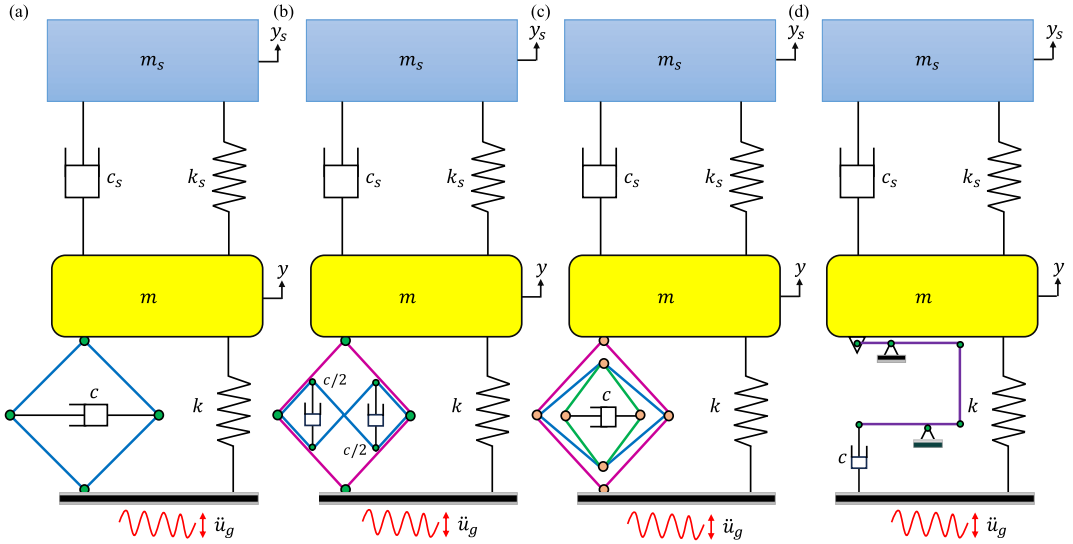

Fig. 9. The structural diagrams of the single degree of freedom systems isolated by the (a) ordinary, (b) compound, (c) nested, and (d) levered damping-amplifier base isolators subjected to base excitation.

the isolator, and $\kappa = \omega/\nu_s$ defines the excitation frequency ratio. The displacement of the SDOF system is obtained as

$$\tilde{Z}_s = \left(\frac{U_s}{U_g}\right)\nu_s^2 = \frac{2\,\mathrm{i}\mu\,\kappa_d\,\kappa\,\xi_d\,\vartheta + \mu\,{\kappa_d}^2}{\tilde{\delta}_f} \tag{46}$$

The displacement of the isolator is obtained as

$$\tilde{Z} = \left(\frac{U}{U_g}\right)\nu_s^2 = \frac{-\mu\,\kappa^2 + \mu + 1 + \mathrm{i}\left(2\,\kappa\,\mu\,\xi_s + 2\,\kappa\,\xi_s\right)}{\tilde{\delta}_f} \tag{47}$$

The denominator of Eqs. (46) and (47) has been obtained as

$$\tilde{\delta}_f = \begin{array}{c} 4\,\kappa^2\mu\,\xi_d\,\xi_s\,\kappa_d\,\vartheta - \kappa^4\mu + \kappa^2\mu\,{\kappa_d}^2 + \mu\,\kappa^2 - \mu\,{\kappa_d}^2 + \kappa^2 \\ +\mathrm{i}\left(2\,\kappa^3\mu\,\xi_d\,\kappa_d\,\vartheta + 2\,\kappa^3\mu\,\xi_s - 2\,\mu\,\kappa_d\,\kappa\,\xi_d\,\vartheta - 2\,\kappa\,\mu\,\xi_s\,{\kappa_d}^2 + 2\,\kappa^3\xi_s\right) \end{array} \tag{48}$$

The isolated structure is subjected to harmonic base excitation. H_∞ optimisation is applicable, and the optimal design parameters of the isolator are derived analytically. The H_∞ optimisation method is employed in this study to derive the optimal design parameters for damping-amplifier base isolators. Although traditionally used in the design of dynamic vibration absorbers (DVAs), the method is well-suited for base isolation systems due to their analogous dynamic structure. Both systems involve two interacting degrees of freedom and aim to minimise the response of the primary structure under dynamic excitation. The H_∞ approach ensures robustness against worst-case excitation scenarios, such as broadband seismic inputs, by minimising the maximum gain of the transfer function from disturbance to response. Furthermore, this method facilitates the derivation of closed-form expressions for optimal damping ratios and frequency tuning, which is essential for analytical insight and efficient parametric design. Its applicability to base isolation has been supported by recent studies in structural dynamics and vibration control. To perform H_∞ optimisation, ξ_s is considered zero, i.e. $\xi_s = 0$, to satisfy its mathematical condition [44] derived below.

$$|\tilde{Z}_s| = \sqrt{\frac{A^2 + \xi_d^2 B^2}{C^2 + \xi_d^2 D^2}} \tag{49}$$

The closed-form expressions for A, B, C, and D are derived and expressed below.

$$\begin{array}{l} A = \mu\,{\kappa_d}^2,\, B = 2\,\kappa_d\,\vartheta\,\mu\,\kappa,\, C = -\kappa^4\mu + \kappa^2\mu\,{\kappa_d}^2 + \kappa^2\mu - \mu\,{\kappa_d}^2 + \kappa^2, \\ \text{and} \quad D = 2\,\kappa^3\mu\,\kappa_d\,\vartheta - 2\,\kappa\,\mu\,\kappa_d\,\vartheta \end{array} \tag{50}$$

Two constraints are derived from Eq. (49) and expressed as

$$\left|\frac{A}{B}\right|_{\kappa_j} = \left|\frac{C}{D}\right|_{\kappa_j} \quad \text{and} \quad \left|\frac{B}{D}\right|_{\kappa_1} = \left|\frac{B}{D}\right|_{\kappa_2} \tag{51}$$

Eq. (50) is substituted in the first expression of Eq. (51).

$$\begin{array}{l} \kappa^4\mu + \left(-2\,\mu\,{\kappa_d}^2 - \mu - 1\right)\kappa^2 + 2\,\mu\,{\kappa_d}^2 = 0 \\ \kappa_1^2 + \kappa_2^2 = \dfrac{2\,\mu\,{\kappa_d}^2 + \mu + 1}{\mu} \end{array} \tag{52}$$

Eq. (50) is substituted in the second expression of Eq. (51).

$$\kappa_1^2 + \kappa_2^2 = 2 \tag{53}$$

Equating Eqs. (52) and (53), the frequency ratio of the damper is derived as

$$\left(\kappa_d\right)_{\mathrm{opt}} = \sqrt{\frac{1-\mu}{2\mu}} \tag{54}$$

The closed-form expressions for $\kappa_{1,2}^2$ have been derived as

$$\kappa_{1,2}^2 = 1 \pm \sqrt{1 - 2\,{\kappa_d}^2} \tag{55}$$

The closed-form expression for the optimal damping ratio of the isolator has been derived using a mathematical expression and is expressed as

$$\left.\frac{\partial|\tilde{Z}_s(\kappa)|^2}{\partial\kappa^2}\right|_{\kappa_{1,2}^2} = 0 \quad \text{and} \quad \left(\xi_d\right)_{\mathrm{opt}} = \sqrt{\frac{\xi_{d1}^2 + \xi_{d2}^2}{2}} \tag{56}$$

Eq. (49) is substituted in the first expression of Eq. (56). The closed-form expression for the damping ratio of the isolator is derived as

$$\begin{array}{l} G_1\xi_d^4 + G_2\xi_d^2 + G_3 = 0 \\ \left(\xi_{d\,1,d2}\right)_{\kappa_{1,2}^2}^2 = \dfrac{-G_2 \pm \sqrt{{G_2}^2 - 4\,G_1\,G_3}}{2G_1} \end{array} \tag{57}$$

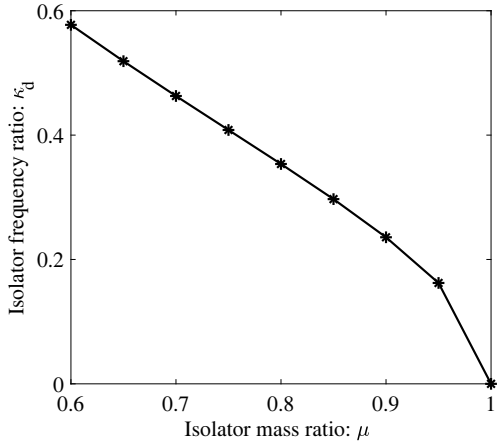

Fig. 10. Variations in the optimal frequency ratio of the isolators as a function of the mass ratio of the isolator.

$$
\begin{aligned}
G_1 &= 16\,\kappa_{1,2}^6\mu^2{\kappa_d}^2\vartheta^4 - 16\,\kappa_{1,2}^4\mu^2{\kappa_d}^2\vartheta^4 \\
&\quad 6\,\kappa_{1,2}^8\mu^2\vartheta^2 + \left(-8\,\mu^2{\kappa_d}^2\vartheta^2 - 8\,\mu^2\vartheta^2 - 8\,\mu\,\vartheta^2\right)\kappa_{1,2}^6 \\
G_2 &= +\left(8\,\mu^2{\kappa_d}^4\vartheta^2 + 8\,\mu^2{\kappa_d}^2\vartheta^2 + 4\,\mu\,{\kappa_d}^2\vartheta^2 + 2\,\mu^2\vartheta^2 + 4\,\mu\,\vartheta^2 + 2\,\vartheta^2\right)\kappa_{1,2}^4 \\
&\quad -8\,\kappa_{1,2}^2\,\mu^2{\kappa_d}^4\vartheta^2 \\
&\quad 2\,\kappa_{1,2}^6\mu^2{\kappa_d}^2 + \left(-3\,\mu^2{\kappa_d}^4 - 3\,\mu^2{\kappa_d}^2 - 3\,\mu\,{\kappa_d}^2\right)\kappa_{1,2}^4 \\
G_3 &= +\left(\mu^2{\kappa_d}^6 + 4\,\mu^2{\kappa_d}^4 + 2\,\mu\,{\kappa_d}^4 + \mu^2{\kappa_d}^2 + 2\,\mu\,{\kappa_d}^2 + {\kappa_d}^2\right)\kappa_{1,2}^2 \\
&\quad -\mu^2{\kappa_d}^6 - \mu^2{\kappa_d}^4 - \mu\,{\kappa_d}^4
\end{aligned}
\tag{58}
$$

The frequency ratio variations are derived using the H_∞ optimisation method. The graphical representations of these variations are determined using Eq. (54) and displayed in Fig. 10. According to this graph, the optimal frequency ratio decreases with the increment of the isolator mass ratio and provides additional flexibility to the isolator with sufficient load-bearing capacity. In addition, the value of the isolator mass ratio should be less than or equal to 0.95, i.e., $\mu \leq 0.95$, to achieve robust vibration reduction capacity from the isolator. Simultaneously, this type of parametric graph is also generated using the Eqs. (57) and (58). Accordingly, the optimal damping ratio changes of each isolator are obtained and shown in Fig. 11. The damping ratio variations for ordinary damping-amplifier base isolator, compound damping-amplifier base isolator, nested damping-amplifier base isolator, and levered damping-amplifier base isolator with respect to the isolator mass ratio are shown in Fig. 11(a)–(d). The isolator damping ratio is a function of the variable isolator mass ratio. In the case of an ordinary damping-amplifier base isolator, the damping ratio progressively rises with increasing damping amplifier angle and falls with increasing isolator mass ratio. The compound damping-amplifier base isolator with the primary damping amplifier angle exhibits the same properties. Section 2.2 states that the secondary damping amplifier angle has a value of 64^o. Furthermore, the nested damping-amplifier base isolator shares the same physical properties of the damping ratio as ordinary and compound isolators. The damping ratio of the isolator is influenced by three amplifier angles: primary, secondary, and tertiary. This graph maintains constant secondary and tertiary angles. Regarding applying the minimal lever arm ratio, the levered damping-amplifier base isolators' characteristics differ slightly from those of the other three isolators. The value of b_1/a_1 is maintained constant, i.e., $b_1/a_1 = 1.0$, to preserve the design's simplicity. b_2/a_2 has a value that ranges from 1 to 3. A greater value of the b_2/a_2 ratio dramatically reduces the ideal damping ratio, making it unsuitable for use as a base isolator. To obtain a strong vibration reduction capacity from the levered damping-amplifier base isolator, a lower value of b_2/a_2 is necessary for its optimal design.

4. Dynamic response evaluation

The dynamic responses of the structures are evaluated to assess the effectiveness of the damping amplifiers in enhancing the vibration reduction performance of the isolators.

4.1. Frequency domain responses

The newly developed damping-amplifier base isolators are applied to the single degree of freedom systems to achieve each one of their vibration reduction performances. The governing system parameters are considered the same for all controlled single degree of freedom systems. The damping ratio of the SDOF system is considered 0.01 and is listed in Table 1. The harmonic excitation is applied at the base of the isolated structures. As a result, the dynamic responses are developed from the isolated structures. The detailed analysis of dynamic response evaluation is illustrated in the following. This vibration reduction capacity is derived for the H_∞ novel isolators. To perform the analytical study, the H_∞ optimised design parameters for the novel isolators are derived using Eq. (54)–(58). The design parameters for the conventional base isolator are obtained from a published journal. The details of all system parameters for optimum novel and conventional base isolators are listed in Table 2. To conduct a fair comparison between the vibration reduction performances of the novel base isolators and the conventional base isolators, the mass ratios of both are kept exactly the same. The differences in the optimal displacements of the single degree of freedom systems isolated by the H_∞ optimised ordinary, compound, nested, and levered damping-amplifier base isolators in relation to the frequency ratio are now obtained and graphically presented in Fig. 12(a)–(d) after all system parameters have been applied. The frequency response function is also used to analytically determine the maximum displacement response of the uncontrolled single-degree-of-freedom system, and the result is 50. The H_∞ optimised ordinary, compound, nested, and levered damping-amplifier base isolators isolated single degree of freedom systems yielded the following maximum displacement responses: 1.3397. The single degree of freedom system isolated by the conventional base isolator yields a maximum displacement response of 8.4918. The vibration reduction capacities of the novel isolators are derived with respect to the conventional base isolator, and the mathematical expression for the required derivation is as follows.

$$
Z_{\mathrm{dr}}(\%) = \left(\frac{\left(\tilde{Z}_s(\kappa)\right)_{\mathrm{conventional}} - \left(\tilde{Z}_s(\kappa)\right)_{\mathrm{novel}}}{\left(\tilde{Z}_s(\kappa)\right)_{\mathrm{conventional}}}\right) \times 100 \tag{59}
$$

where $Z_{\mathrm{dr}}(\%)$ defines the displacement reduction capacity of the novel isolator compared to the conventional one. $\left(\tilde{Z}_s(\kappa)\right)_{\mathrm{conventional}}$ and $\left(\tilde{Z}_s(\kappa)\right)_{\mathrm{novel}}$ define the maximum displacements of the SDOF systems isolated by the conventional and the novel base isolators. Using Eq. (59), the vibration reduction capacities of the suggested isolators are calculated in relation to the conventional base isolator. As a result, the H_∞ optimised ordinary, compound, nested, and levered damping-amplifier base isolators are 84.22 % more capable of reducing vibration than the conventional base isolator. The structural acceleration of the superstructure is further obtained to comprehensively evaluate the control performance of the proposed damping amplifier-based isolators. Accordingly, the variations in the optimal accelerations of the structures isolated by the optimum ODABI, CDABI, NDABI, and LDABI as a function of the frequency ratio are shown in Fig. 13(a)–(d). The maximum structural acceleration of the SDOF system isolated by conventional BI is derived as 2.0358, while the maximum structural acceleration of the SDOF system isolated by the novel base isolator is derived as 1.6122.

$$
Z_{\mathrm{ar}}(\%) = \left(\frac{\left(\ddot{\tilde{Z}}_s(\kappa)\right)_{\mathrm{conventional}} - \left(\ddot{\tilde{Z}}_s(\kappa)\right)_{\mathrm{novel}}}{\left(\ddot{\tilde{Z}}_s(\kappa)\right)_{\mathrm{conventional}}}\right) \times 100 \tag{60}
$$

where $Z_{\mathrm{ar}}(\%)$ defines the acceleration reduction capacity of the novel isolator compared to the conventional one. $\left(\ddot{\tilde{Z}}_s(\kappa)\right)_{\mathrm{conventional}}$ and

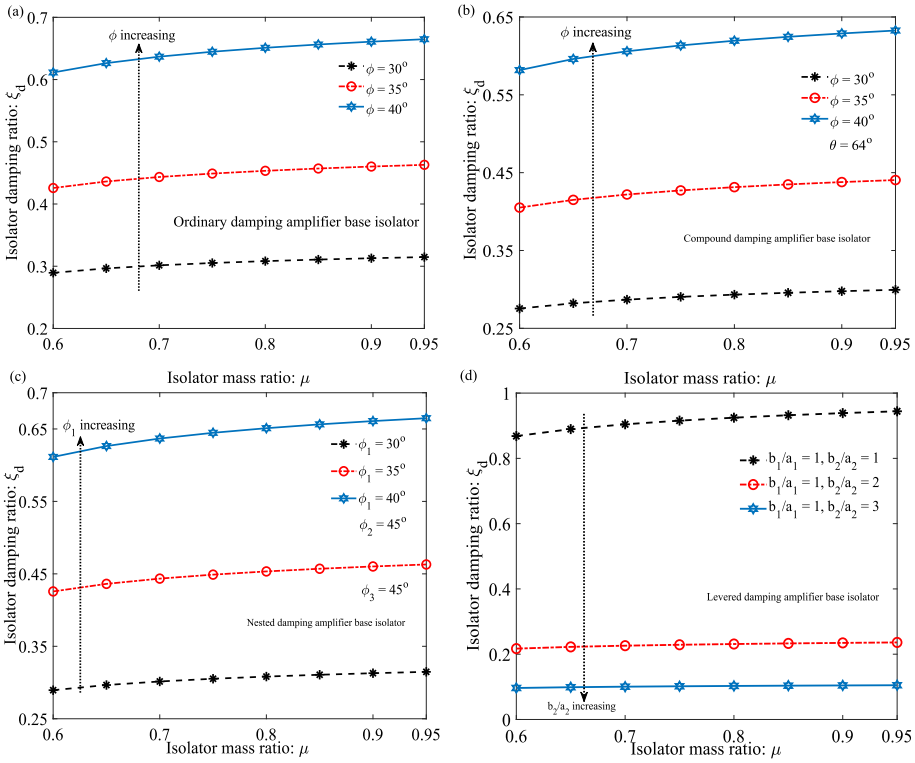

Fig. 11. Variations in the optimal damping ratio of the (a) ordinary, (b) compound, (c) nested, and (d) levered damping-amplifier base isolators as a function of the mass ratio of the isolator.

Table 1
The structural system parameter for the single degree of freedom system.

Primary structure	Governing system parameter	Value ξ_s
Single degree of freedom system	Damping ratio	0.01

$\left(\ddot{Z}_s(\kappa)\right)_{\text{novel}}$ define the maximum accelerations of the SDOF systems isolated by the conventional and the novel base isolators. The maximum values are substituted in Eq. (60) to obtain the acceleration reduction capacity of the novel isolator over the conventional isolator. Accordingly, the novel isolators are 20.81 % superior to the conventional base isolator.

The displacement of each isolator is obtained to further evaluate the efficiency of the novel isolator over the conventional base isolator. The variations in the optimal displacement of the ODABI, CDABI, NDABI, and LDABI as a function of the frequency ratio are shown in Fig. 14(a)–(d). The maximum displacement of the conventional base isolator is obtained as 67.36, while the novel isolator's maximum displacement is obtained as 38.63. Accordingly, the isolator displacement reduction capacity of the novel isolators is significantly 42.65 % superior to the conventional isolator. It is also shown that damping amplifiers reduce base displacement while mitigating the main structural movements, thereby protecting the base layer from vibration-induced damage. The acceleration of each isolator is obtained to further evaluate the efficiency of the novel isolator over the conventional base isolator. The variations in the optimal acceleration of the ODABI, CDABI, NDABI, and LDABI as a function of the frequency ratio are shown in Fig. 15(a)–(d). The maximum acceleration of the conventional base isolator is obtained as 7.4926, while the novel isolator's maximum acceleration is obtained as 1.0256. Accordingly, the isolator acceleration reduction capacity of the novel isolators is significantly 86.31 % superior to the conventional isolator. It is also shown that damping amplifiers reduce base acceleration while mitigating the main structural movements, thereby protecting the base layer from vibration-induced damage.

Table 2
The governing system parameters for the H_∞ optimised conventional and novel base isolators.

System	Introduced by	H_∞ optimisation	
		κ_d	ξ_d
Ordinary damping-amplifier base isolator	This study	0.235702	0.660887
Compound damping-amplifier base isolator	This study	0.235702	0.628856
Nested damping-amplifier base isolator	This study	0.235702	0.660887
Levered damping-amplifier base isolator	This study	0.235702	0.938643
Conventional base isolator	Matsagar and Jangid [45]	0.50	0.10

Conventional base isolator: isolator mass ratio (μ_b) = 0.90, Ordinary damping-amplifier base isolator: $\mu = 0.90$, $\phi = 40^o$; Compound damping-amplifier base isolator: $\mu = 0.90$, $\phi = 40^o$, $\theta = 64^o$; Nested damping-amplifier base isolator: $\mu = 0.90$, $\phi_1 = 40^o$, $\phi_2 = 45^o$, $\phi_3 = 45^o$, and Levered damping-amplifier base isolator: $\mu = 0.90$, $b_1/a_1 = 1$, $b_2/a_2 = 1$. These parameters are applied to the Eq. (54)–(58) to obtain each H_∞ optimised base isolator's optimal natural frequency and damping ratio.

4.2. Time history results

The earthquake records are applied as base excitation to the isolated structures for performing the time history analysis. The Newmark-beta method is employed to perform this analysis. The mass of the SDOF system is considered to be 3000 tons. The time period is 0.5 sec. The earthquakes are downloaded from PEER Berkeley and listed in Table 3. The above-mentioned earthquakes are employed to obtain the response spectra of each earthquake record. Further, the response spectra graph

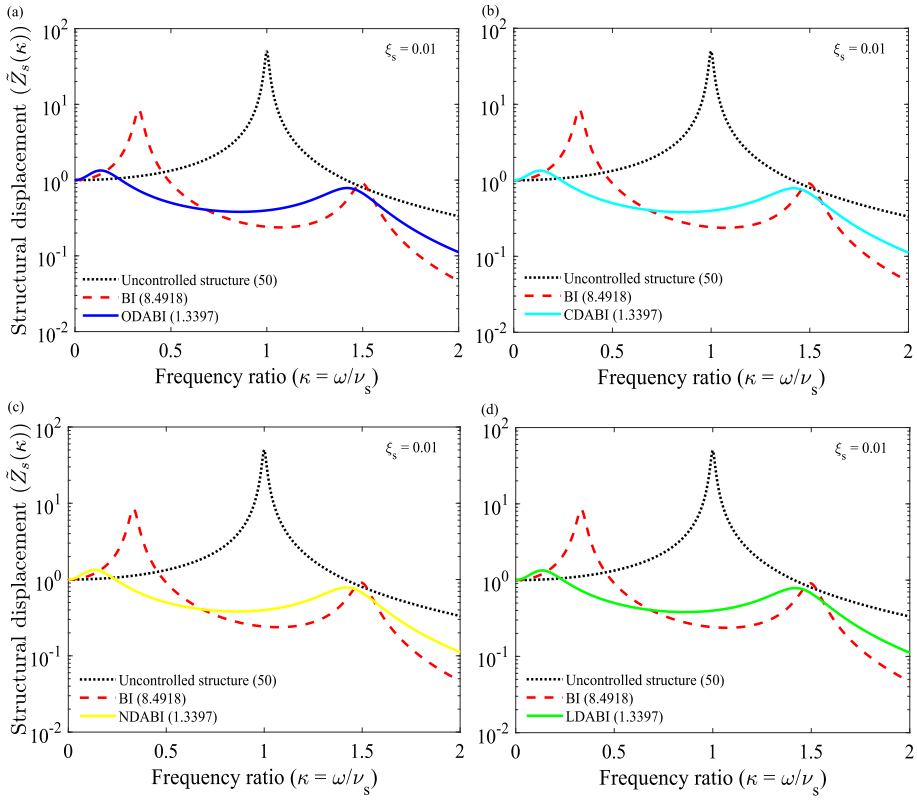

Fig. 12. The variations in the optimal displacements of the structures isolated by the optimum (a) ODABI, (b) CDABI, (c) NDABI, and (d) LDABI as a function of the frequency ratio.

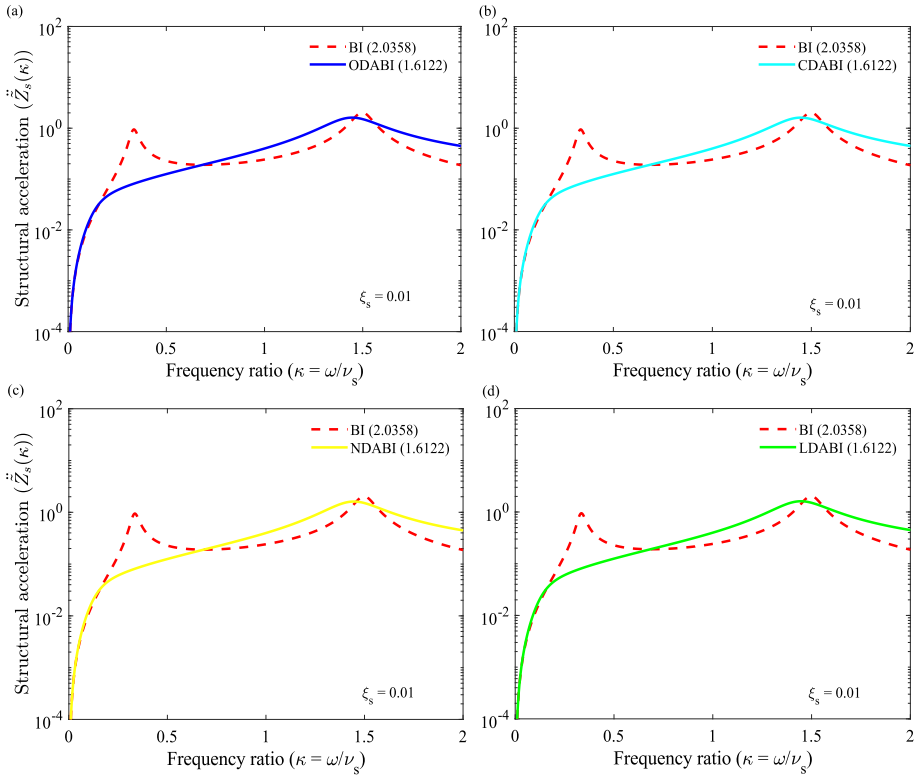

Fig. 13. The variations in the optimal accelerations of the structures isolated by the optimum (a) ODABI, (b) CDABI, (c) NDABI, and (d) LDABI as a function of the frequency ratio.

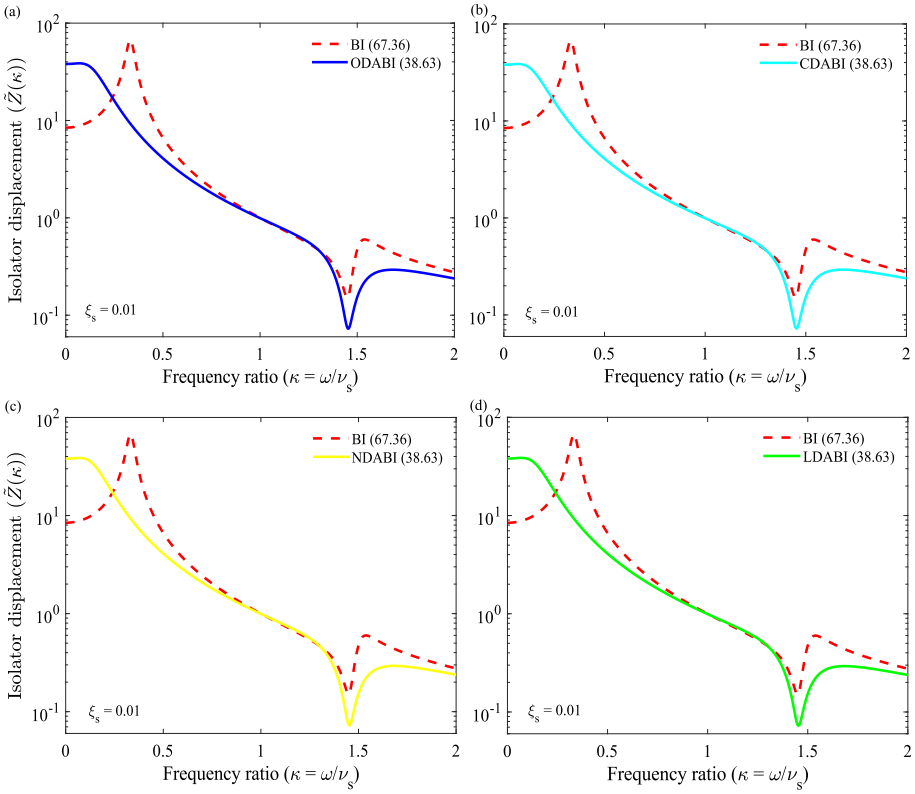

Fig. 14. The variations in the optimal displacement of the (a) ODABI, (b) CDABI, (c) NDABI, and (d) LDABI as a function of the frequency ratio.

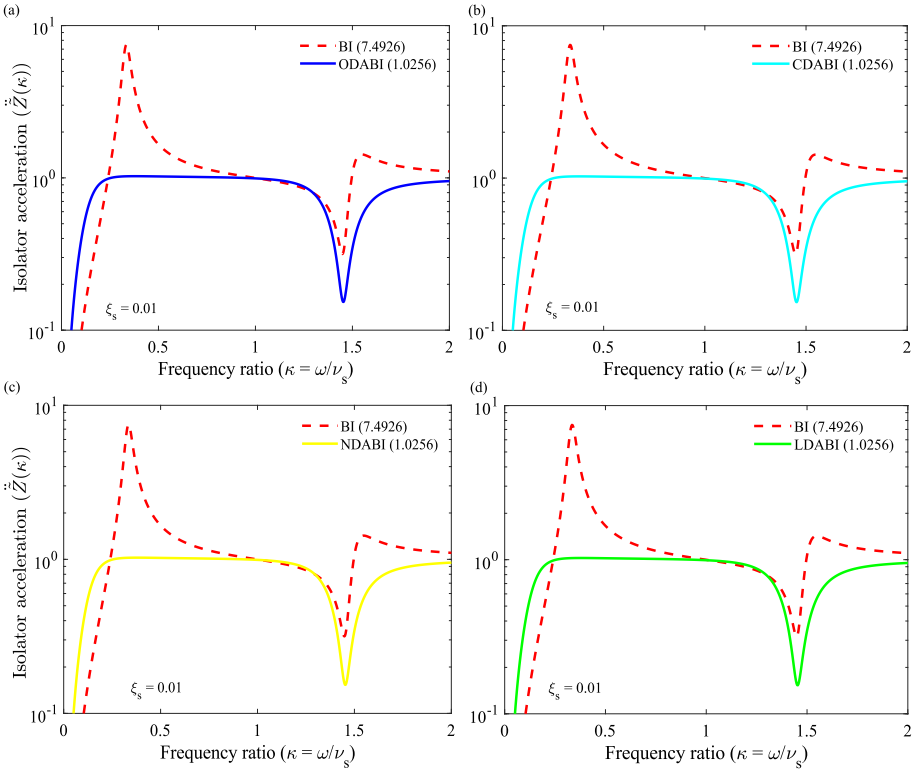

Fig. 15. The variations in the optimal acceleration of the (a) ODABI, (b) CDABI, (c) NDABI, and (d) LDABI as a function of the frequency ratio.

Table 3
Details of earthquake records.

Earthquake	Year	M_w	Recording station	Vs_{30} (m/s)	Component	E_s (km)	PGA,g
Northridge	1994	6.7	Beverly Hills - Mulhol	356	MUL009	13.3	0.52
Duzce, Turkey	1999	7.1	Bolu	326	BOL090	41.3	0.82
Hector Mine	1999	7.1	Hector	685	HEC000	26.5	0.34
Imperial Valley	1979	6.5	Delta	275	H-DLT352	33.7	0.35
Kobe, Japan	1995	6.9	Nishi-Akashi	609	NIS090	8.7	0.51
Kocaeli, Turkey	1999	7.5	Duzce	276	DZC270	98.2	0.36
Landers	1992	7.3	Yermo Fire Station	354	YER270	86	0.24
Loma Prieta	1989	6.9	Capitola	289	CAP090	9.8	0.53
Manjil, Iran	1990	7.4	Abbar	724	ABBAR–T	40.4	0.51
Superstition Hills	1987	6.5	El Centro Imp. Co.	192	B-ICC090	35.8	0.36
Cape Mendocino	1992	7.0	Rio Dell Overpass	312	RIO270	22.7	0.55
Chi-Chi, Taiwan	1999	7.6	CHY101	259	CHY101-N	32	0.44
San Fernando	1971	6.6	LA - Hollywood Stor	316	PEL180	39.5	0.21

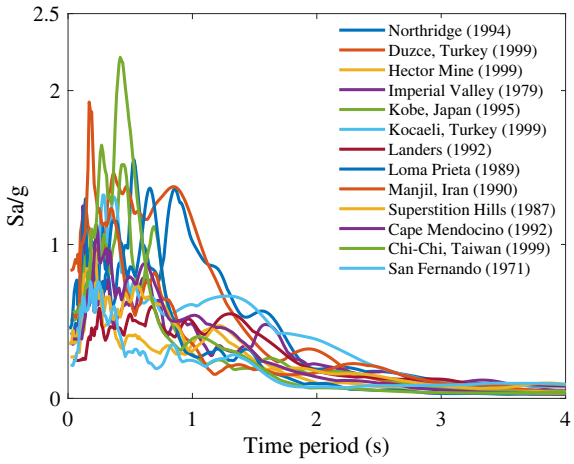

Fig. 16. Response spectra of the earthquake ground motion records. 5 % damping is considered to achieve this plot.

is employed to understand the characteristics of the earthquakes, which are observed from the graph shown in Fig. 16. The nature of the isolated SDOF systems can also be understood from this graph. The numerical analysis is performed for all earthquakes, but the graphs for the Northridge earthquake are shown as the nature of all the graphs is the same. Only the values are different. Accordingly, the variations of the displacements of the SDOF systems isolated by conventional BI, ODABI, CDABI, NDABI, and LDABI, subjected to the Northridge earthquake, are shown in Fig. 17(a)–(d). The damping ratio of the main structure is considered to be 0.02. The maximum displacement of the uncontrolled structure is 0.0106 m, while the maximum displacement of the SDOF system isolated by conventional BI is derived as 0.0058 m. The maximum displacement of the SDOF system isolated by the novel isolator is derived as 0.0014 m. The maximum values are utilised to obtain the displacement reduction capacity of the novel isolators compared to the conventional BI. As a result, the displacement reduction capacity of the novel isolators is significantly 75.86 % superior to the conventional BI. The maximum displacements of uncontrolled structures and structures isolated by conventional and novel base isolators are derived for all considered earthquakes. The values are listed in Table 4. According to the Table 4, the displacement reduction capacity of novel isolators is significantly 67.60 % superior to conventional base isolators. The acceleration reduction capacity of the novel isolator is also determined to evaluate the efficiency of the damping amplifiers compared to the conventional isolator. Accordingly, the variations of the accelerations of the SDOF systems isolated by conventional BI, ODABI, CDABI, NDABI, and LDABI, subjected to the Northridge earthquake, are shown in Fig. 18(a)–(d). The maximum acceleration of the uncontrolled structure is obtained as 1.5868 m/s^2. The maximum acceleration of the SDOF system isolated by the conventional BI is derived as 0.2566 m/s^2. In addition, the novel isolator-controlled SDOF system has a maximum acceleration of 0.1466 m/s^2. The maximum values are utilised to obtain the acceleration reduction capacity of the novel isolators compared to the conventional BI. As a result, the acceleration reduction capacity of the novel isolators is significantly 42.86 % superior to the conventional BI. The maximum accelerations of uncontrolled structures and structures isolated by conventional and novel base isolators are derived for all considered earthquakes. The values are listed in Table 5. According to the Table 5, the acceleration reduction capacity of novel isolators is significantly 33.62 % superior to conventional base isolators. The damping force of the main structure is also mitigated by the isolators. Interestingly, the novel isolators dissipate the damping force more compared to the conventional BI, which are clearly observed in Fig. 19(a)–(d). Fig. 19 presents a phase-plane analysis of structural damping force versus structural displacement for various base-isolated single-degree-of-freedom (SDOF) systems subjected to the Northridge earthquake, with a damping ratio of $\xi_s = 0.02$. Each subplot compares the hysteretic response of an uncontrolled system, a system with conventional base isolation (BI), and a system using a specific advanced base isolation strategy: ODABI, CDABI, NDABI, and LDABI. The elliptical loops in the plots represent energy dissipation characteristics and structural response behaviours. The uncontrolled system consistently exhibits the largest elliptical loops, indicating high energy input and structural demand. Conventional BI reduces this response; however, the red hysteresis loops for BI still display a wide spread, signifying significant damping force and displacement interactions. In contrast, the advanced BI strategies, represented in blue, demonstrate tightly clustered and smaller loops, denoting improved control and reduced dynamic response. ODABI (Fig. 19(a)) effectively narrows the loop area through parameter optimisation, resulting in enhanced energy absorption with lower damping forces. CDABI (Fig. 19(b)) further improves this response by introducing controlled damping, which enables real-time adaptability to seismic inputs and results in even more compact hysteresis loops, suggesting superior mitigation of both displacement and force demands. NDABI (Fig. 19(c)) achieves the best performance among all strategies, as its nonlinear damping model accommodates variations in amplitude and frequency content, allowing for more tailored energy dissipation. The loops under NDABI are the most confined, indicating the highest efficiency in vibration control. LDABI (Fig. 19(d)), while superior to conventional BI, exhibits slightly wider loops than NDABI or CDABI, reflecting the limitations of linear damping in responding to nonlinear seismic excitations. Overall, the advanced BI strategies significantly improve structural resilience by tailoring the force-displacement relationship, with NDABI and CDABI standing out due to their dynamic adaptability and enhanced damping efficiency.

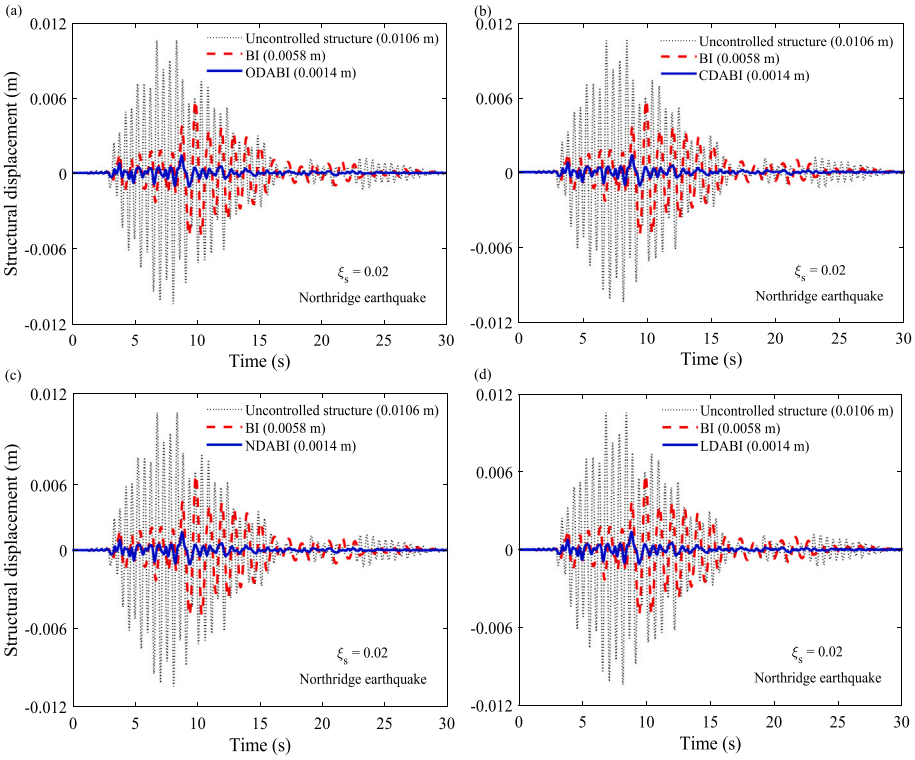

Fig. 17. The variations of the displacements of the SDOF systems isolated by conventional BI, (a) ODABI, (b) CDABI, (c) NDABI, and (d) LDABI, subjected to the Northridge earthquake.

Table 4
Displacement reduction (%) of the novel isolators with respect to the conventional base isolator. The displacements of the uncontrolled and isolated structures are listed in this Table.

Earthquake	Displacement (m)			Displacement reduction (%)
	Uncontrolled	BI	Novel BI	Novel BI
Northridge	0.0106	0.0058	0.0014	76.4472
Duzce, Turkey	0.0133	0.0045	0.0014	68.6909
Hector Mine	0.0037	0.0027	5.10×10^{-4}	80.9658
Imperial Valley	0.0063	0.0023	7.89×10^{-4}	66.4314
Kobe, Japan	0.0187	0.0019	0.0011	42.1201
Kocaeli, Turkey	0.0054	0.0042	0.0013	68.8364
Landers	0.0045	0.0019	4.22×10^{-4}	77.7884
Loma Prieta	0.0066	0.0034	0.0014	57.3697
Manjil, Iran	0.0095	0.0028	0.0012	58.5335
Superstition Hills	0.004	0.0026	7.66×10^{-4}	70.4424
Cape Mendocino	0.006	0.0035	0.001	69.9785
Chi-Chi, Taiwan	0.0094	0.0048	0.0013	72.3731
San Fernando	0.0022	0.0016	5.09×10^{-4}	68.8563
Mean	0.007707692	0.003230769	0.001007344	67.60259231
Standard deviation	0.004549993	0.001279573	0.00036792	10.16115305
Maximum	0.0187	0.0058	0.0014	80.9658
Minimum	0.0022	0.0016	0.00042167	42.1201

5. Summary and conclusions

The manipulation of damping is fundamental to vibration control. This paper discusses four competing damping amplifier device concepts through which the effective damping of an SDOF system can be augmented. The novel designs are summarised in Fig. 20 along with their damping amplification factors and necessary parameter regimes. The four damping amplifiers are termed (1) the ordinary, (2) the compound, (3) the nested, and (4) the levered, based on their geometric configurations. The ordinary damping amplifier is similar to the conventional scissor mechanisms and the X-shaped structures. The amplification factors for all four amplifiers were derived in closed form using the dynamics of the mechanisms. The newly developed damping amplifiers are further applied to classical passive vibration isolation systems to enhance their vibration reduction capacities and overcome their existing limitations. Three novel classes of damping-amplifier vibration isolation systems are introduced. These dampers are applied to structures to control their vibrations. The H_∞ optimisation methods are employed to derive the exact closed-form expression for the optimal design parameters of these novel dampers. A parametric study is performed using these optimal closed-form solutions for the dampers. The vibration reduction capacities of the H_∞ optimised novel dampers are compared with the vibration reduction capacities of the optimum conventional base isolators.

Moving from the ordinary to the compound and the nested designs represents an increasing damping amplification with a suitable choice of

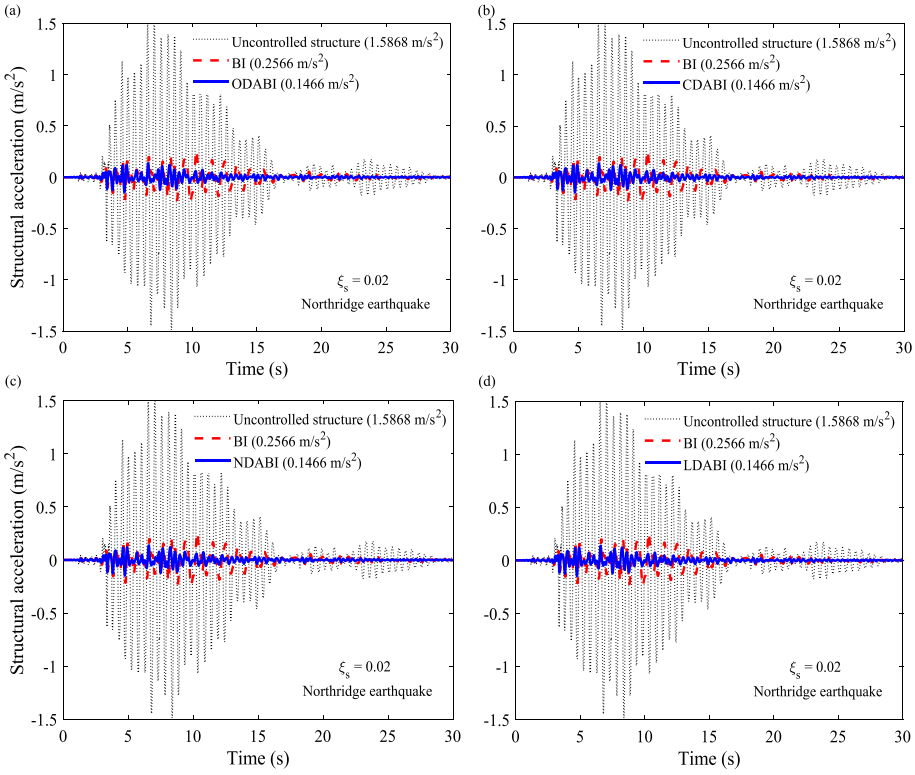

Fig. 18. The variations of the accelerations of the SDOF systems isolated by conventional BI, (a) ODABI, (b) CDABI, (c) NDABI, and (d) LDABI, subjected to the Northridge earthquake.

Table 5
Acceleration reduction (%) of the novel isolators with respect to the conventional base isolator. The accelerations of the uncontrolled and isolated structures are listed in this Table.

Earthquake	Acceleration (m/s^2)			Acceleration reduction (%)
	Uncontrolled	BI	Novel BI	Novel BI
Northridge	1.5868	0.2566	0.1466	42.8629
Duzce, Turkey	2.0829	0.6064	0.4516	25.5157
Hector Mine	0.5778	0.1516	0.0877	42.1532
Imperial Valley	0.9541	0.202	0.1091	45.9926
Kobe, Japan	2.9145	0.3329	0.2544	23.5769
Kocaeli, Turkey	0.8928	0.3902	0.2436	37.5704
Landers	0.6171	0.1391	0.0799	42.5134
Loma Prieta	1.1414	0.4446	0.3753	15.591
Manjil, Iran	1.6129	0.3017	0.2553	15.3906
Superstition Hills	0.6674	0.2063	0.1447	29.8737
Cape Mendocino	0.9449	0.2826	0.1694	40.0364
Chi-Chi, Taiwan	1.3278	0.3212	0.1786	44.4056
San Fernando	0.4645	0.1682	0.1151	31.6017
Mean	1.214223077	0.292569231	0.200869231	33.62185385
Standard deviation	0.696880142	0.132160164	0.112454186	10.82255811
Maximum	2.9145	0.6064	0.4516	45.9926
Minimum	0.4645	0.1391	0.0799	15.3906

parameters as shown in Fig. 20. The graphical illustrations provided in the paper further clarify the role of different mechanism parameters in damping amplification. This work's impact lies in amplifying a conventional damper's attenuation effects through specially designed geometric configurations. The paper presents:

1. Four competing damping amplifier designs: ordinary, compound, nested, and levered, characterised by their distinct geometric arrangements. Damping amplifications of orders of magnitude are possible with physically realistic parameter values.
2. Analytical derivations of the amplification factors achieved by each design through closed-form dynamic analysis of the underlying mechanisms.
3. An analytical parameter analysis to explicitly establish a hierarchy of damping amplification through the four concepts.
4. Three new classes of damping-amplifier vibration isolation systems.
5. Analytical H_∞ optimisation techniques to determine optimal design parameters for damping-amplifier base isolators using closed-form expressions.

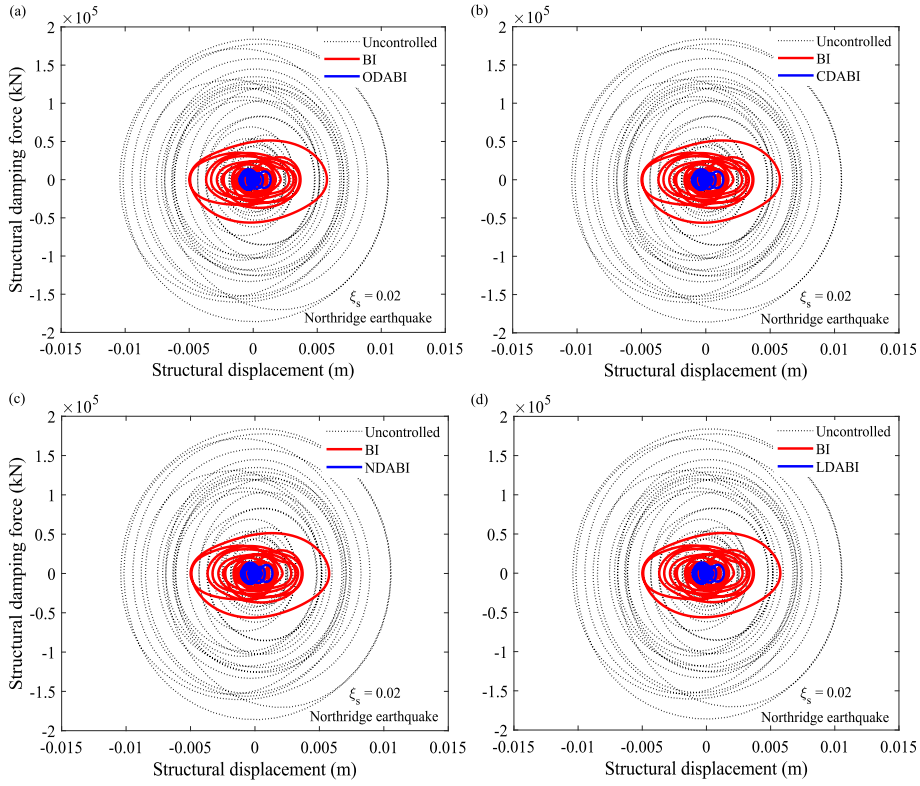

Fig. 19. The damping forces of the SDOF systems isolated by conventional BI, (a) ODABI, (b) CDABI, (c) NDABI, and (d) LDABI, subjected to the Northridge earthquake.

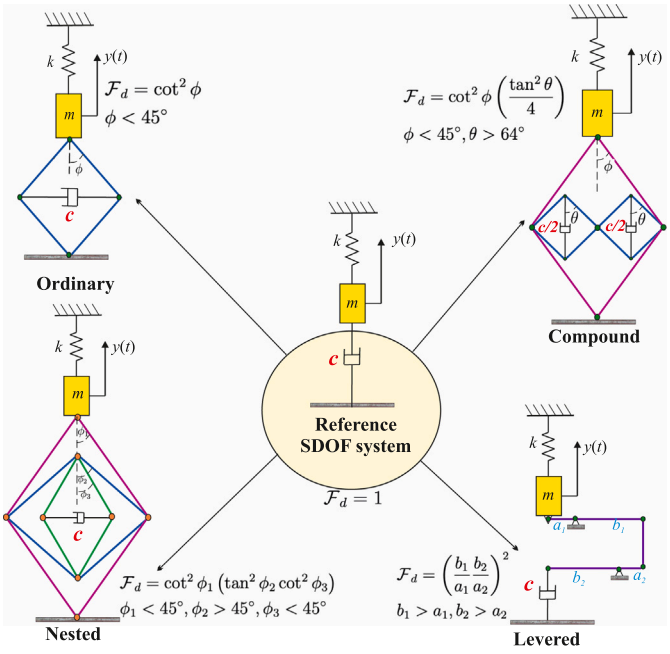

Fig. 20. Summary of the four novel amplifiers, their corresponding damping amplification factors ($\mathcal{F}_d$), and necessary parameter regimes. All amplifiers use the same amount of damping as the reference SDOF oscillator.

6. A parametric study using these optimal closed-form solutions for the dampers, demonstrating higher isolator mass ratios to achieve robust performances.
7. Frequency and time domain analyses are performed to obtain the dynamic response reduction capacity of the novel isolators compared to the conventional base isolators. Comparative numerical analysis shows an 84.22 % respective improvement in vibration reduction over conventional base isolators.

The analytical formulation presented here is about damping. However, the scope of the amplifier designs conceived here can go beyond the damping enhancement. The novel mechanical setups can be inverted to achieve an incredible advantage in active control. By replacing the dampers with actuators and reversing the mechanism angles, a small control force can be amplified to deliver a superior control framework for the underlying dynamic system. All four amplifiers can be used for enhanced vibration energy harvesting by swapping the dampers with suitable piezoelectric units. By miniaturising the mechanisms and including many unit cells in a periodic manner, it will be possible to create a designer ultra-high-damping metamaterial. Such an ultra-high-damping metamaterial can attenuate vibration under a broad range of situations, as the material can be designed from the bottom up. Future research is also necessary on how the novel damping amplifiers can be used for vibration isolation and vibration absorption for multi-degree-of-freedom systems with a wide range of dynamic forces, such as wind and earthquake excitations.

CRediT authorship contribution statement

Sondipon Adhikari: Writing – review & editing, Writing – original draft, Visualization, Validation, Supervision, Software, Resources, Project administration, Methodology, Investigation, Formal analysis, Data curation, Conceptualization. **Sudip Chowdhury:** Writing – review & editing, Writing – original draft, Validation, Software, Resources, Methodology, Investigation, Funding acquisition, Formal analysis, Data curation, Conceptualization.

Declaration of competing interest

The authors declare that they have no known competing financial interests or personal relationships that could have appeared to influence the work reported in this paper.

Acknowledgement

Sudip Chowdhury would like to acknowledge the postdoctoral research grant received from the University of Glasgow for the financial support for this research work.

Data availability

All data, models, and code generated or used during the study appear in the submitted article.

References

[1] Smith MC. Synthesis of mechanical networks: the inerter. IEEE Trans Autom Control 2002;47(10):1648–62.
[2] Song J, Bi K, Ma R, Wang Z, Xu K, Hao H. Vibration control of adjacent structures equipped with inerter-based dampers considering nonlinearities: analytical and experimental studies. Mech Syst Signal Process 2024;206:110903.
[3] Li Z, Xu K, Wang Z, Bi K, Qin H, Giaralis A. Analytical design of non-grounded tuned mass-damper-inerter for base-excited structures. Int J Mech Sci 2024;276:109394.
[4] Chillemi M, Furtmüller T, Adam C, Pirrotta A. Fluid inerter-based vibration control of multi-modal structures subjected to vertical vibration. Eng Struct 2024;307:117938.
[5] Farsijani D, Gholam S, Karampour H, Talebian N. The impact of the frequency content of far-field earthquakes on the optimum parameters and performance of tuned mass damper inerter. Structures 2024;60:105925. Elsevier.
[6] Yang X, Zhang T, Shen Y, Liu Y, Bui V, Qiu D. Tradeoff analysis of the energy-harvesting vehicle suspension system employing inerter element. Energy 2024;308:132841.
[7] Kuhnert WM, Gonçalves PJP, Ledezma-Ramirez DF, Brennan MJ. Inerter-like devices used for vibration isolation: a historical perspective. J Franklin Inst 2020.
[8] Wang B, Xu F, Zhang M. Experimental and numerical study of a novel low-frequency tuned mass damper-inerter. Eng Struct 2025;331:119980.
[9] Khorsand S, Rofooei FR. H_∞ optimum design and nonlinear seismic performance assessment of tuned-mass-damper-inerter (TMDI) supported by an auxiliary structure. Structures 2024;69:107257. Elsevier.
[10] Marian L, Giaralis A. The tuned mass-damper-inerter for harmonic vibrations suppression, attached mass reduction, and energy harvesting. Smart Struct Syst 2017;19(6):665–78.
[11] Lazar IF, Neild SA, Wagg DJ. Using an inerter-based device for structural vibration suppression. Earthq Eng Struct Dyn 2014;43(8):1129–47.
[12] Sun F, Xiao L. Bandgap characteristics and seismic applications of inerter-in-lattice metamaterials. J. Eng. Mech. 2019;145(9):04019067.
[13] Zhang R, Wu M, Zhao Z, Tang Y. Structural state nonlinearity-based design and modification formulae of inerter-based systems. Soil Dyn Earthq Eng 2024;187:108946.
[14] Song Y, Chen L, Yang T. Geometrically nonlinear inerter for vibration suppression. Appl Math Mech 2023;44(11):1871–86.
[15] Cheng Z, Palermo A, Shi Z, Marzani A. Enhanced tuned mass damper using an inertial amplification mechanism. J Sound Vib 2020;475:115267.
[16] Chowdhury S, Banerjee A, Adhikari S. The nonlinear negative stiffness inertial amplifier base isolators for dynamic systems. Mech Based Des Struct Mach 2024:1–40.
[17] Chowdhury S, Banerjee A, Adhikari S. A critical review on inertially-amplified passive vibration control devices. Arch Comput Methods Eng 2024:1–37.
[18] C. Yilmaz, G. M. Hulbert, N. Kikuchi, Phononic band gaps induced by inertial amplification in periodic media, Phys Rev B—Condens Matter Mater Phys 76 (5) (2007) 054309.
[19] Chowdhury S, Banerjee A, Adhikari S. Enhancing seismic resilience of nonlinear structures through optimally designed additional mass dampers. Int J Non Linear Mech 2024:104717.
[20] Chowdhury S, Banerjee A, Adhikari S. Nonlinear inertial amplifier resilient friction base isolators for multiple degrees of freedom systems. Mech Adv Mater Struct 2023:1–8.
[21] Chowdhury S, Banerjee A. The impacting vibration absorbers. Appl Math Model 2024;127:454–505.
[22] Acar G, Yilmaz C. Experimental and numerical evidence for the existence of wide and deep phononic gaps induced by inertial amplification in two-dimensional solid structures. J Sound Vib 2013;332(24):6389–404.
[23] Frandsen NMM, Bilal OR, Jensen JS, Hussein MI. Inertial amplification of continuous structures: large band gaps from small masses. J Appl Phys 2016;119(12):124902.
[24] Valvano S, Alaimo A, Orlando C. Higher-order models for the passive damping analysis of variable-angle-tow composite plates. Comput Struct 2023;280:106992.
[25] Adhikari S. Damping models for structural vibration [Ph.D. thesis]. Cambridge, UK: Cambridge University Engineering Department; 2000 Sep.
[26] Adhikari S. Qualitative dynamic characteristics of a non-viscously damped oscillator. Proc R Soc Lond Ser A 2005;461(2059):2269–88.
[27] Adhikari S, Pascual B. Eigenvalues of linear viscoelastic systems. J Sound Vib 2009;325(4–5):1000–11.
[28] Batou A, Adhikari S. Optimal parameters of viscoelastic tuned-mass dampers. J Sound Vib 2019;445(4):17–28.
[29] Biot MA. Variational principles in irreversible thermodynamics with application to viscoelasticity. Phys Rev E 1955;97(6):1463–69.
[30] Biot MA. Linear thermodynamics and the mechanics of solids. In: Proceedings of the third U. S. national congress on applied mechanics; New York: ASME; 1958. p. 1–18.
[31] Adhikari S. Structural dynamic analysis with generalized damping models: analysis. UK: Wiley ISTE; 2013. (368 pages). http://eu.wiley.com/WileyCDA/WileyTitle/productCd-1848215215.html.
[32] Lázaro M, Pérez-Aparicio JL. Multiparametric computation of eigenvalues for linear viscoelastic structures. Comput Struct 2013;117:67–81.
[33] Bagley RL, Torvik PJ. Fractional calculus–a different approach to the analysis of viscoelastically damped structures. AIAA J 1983;21(5):741–48.
[34] Golla DF, Hughes PC. Dynamics of viscoelastic structures–a time domain finite element formulation. ASME J Appl Mech 1985;52:897–906.
[35] McTavish DJ, Hughes PC. Modeling of linear viscoelastic space structures. ASME J Vib Acoust 1993;115:103–10.
[36] Hwang J-S, Huang Y-N, Hung Y-H. Analytical and experimental study of toggle-brace-damper systems. J Struct Eng 2005;131(7):1035–43.
[37] Feng H, Zhou F, Ge H, Zhu H, Zhou L. Energy dissipation enhancement through multi-toggle brace damper systems for mitigating dynamic responses of structures. Structures 2021;33:2487–99. Elsevier.
[38] Constantinou MC, Tsopelas P, Hammel W, Sigaher AN. Toggle-brace-damper seismic energy dissipation systems. J Struct Eng 2001;127(2):105–12.
[39] Şigaher AN, Constantinou MC. Scissor-jack-damper energy dissipation system. Earthq Spectra 2003;19(1):133–58.
[40] Rama Raju K, Jame A, Gopalakrishnan N, Muthumani K, Iyer NR. Experimental studies on seismic performance of three-storey steel moment resisting frame model with scissor-jack-magnetorheological damper energy dissipation systems. Struct Control Health Monit 2014;21(5):741–55.
[41] Walsh KK, Cronin KJ, Rambo-Roddenberry MD, Grupenhof K. Dynamic analysis of seismically excited flexible truss tower with scissor-jack dampers. Struct Control Health Monit 2012;19(8):723–45.
[42] Yang X-L, Xiang Y, Li G-Q, Li H-F, Cui Y-Q. Novel scissor-jack-damper with spatial configuration and enhanced efficiency. Struct Des Tall Spec Build 2025;34(4):e70008.
[43] Baquero Mosquera JS, Almazán JL, Tapia NF. Amplification system for concentrated and distributed energy dissipation devices. Earthq Eng Struct Dyn 2016;45(6):935–56.
[44] J. Den Hartog. Mechanical vibrations. 4th ed. New York:McGraw-Hill Book Company, Inc.; 1956.
[45] Matsagar VA, Jangid RS. Seismic response of base-isolated structures during impact with adjacent structures. Eng Struct 2003;25(10):1311–23.